

Molecular characterization of DXCF
cyanobacteriochromes from the cyanobacterium
Acaryochloris marina identifies a blue-light power
sensor

メタデータ	言語: en 出版者: American Society for Biochemistry and Molecular Biology 公開日: 2018-01-11 キーワード (Ja): キーワード (En): 作成者: Hasegawa, Masumi, Fushimi, Keiji, Miyake, Keita, Nakajima, Takahiro, Oikawa, Yuki, Enomoto, Gen, Sato, Moritoshi, Ikeuchi, Masahiko, Narikawa, Rei メールアドレス: 所属:
URL	http://hdl.handle.net/10297/00024383

**Molecular characterization of DXCF cyanobacteriochromes from the cyanobacterium
Acaryochloris marina identifies a blue-light power sensor**

Masumi Hasegawa¹, Keiji Fushimi^{1,3}, Keita Miyake¹, Takahiro Nakajima², Yuki Oikawa¹, Gen Enomoto^{2,3}, Moritoshi Sato², Masahiko Ikeuchi^{2,3}, Rei Narikawa^{1,3,4}

¹Department of Biological Science, Faculty of Science, Shizuoka University, Ohya, Suruga-ku, Shizuoka 422-8529, Japan. ²Graduate School of Arts and Sciences, University of Tokyo, Komaba, Meguro, Tokyo 153-8902, Japan. ³Core Research for Evolutional Science and Technology, Japan Science and Technology Agency, 4-1-8 Honcho Kawaguchi, Saitama 332-0012 Japan. ⁴Green Biology Research Division, Research Institute of Green Science and Technology, Shizuoka University, Ohya, Suruga-ku, Shizuoka 422-8529, Japan.

Running title: DXCF cyanobacteriochromes from *Acaryochloris marina*

*To whom correspondence should be addressed.

Email: narikawa.rei@shizuoka.ac.jp, Tel: +81-54-238-4783

Keywords: cyanobacteria; photobiology; photoreceptor; site-directed mutagenesis; spectroscopy; cyanobacteriochrome; phytochrome

ABSTRACT

Cyanobacteriochromes (CBCRs) are linear tetrapyrrole-binding photoreceptors that sense a wide range of wavelengths from ultraviolet to far-red. The primary photoreaction in these reactions is a *Z/E* isomerization of the double bond between rings C and D. After this isomerization, various color-tuning events establish distinct spectral properties of the CBCRs. Among the various CBCRs, the DXCF CBCR lineage is widely distributed among cyanobacteria. Because the DXCF CBCRs from the cyanobacterium *Acaryochloris marina* vary widely in sequence, we focused on these CBCRs in this study. We identified seven DXCF CBCRs in *A. marina* and analyzed them after isolation from *Escherichia coli* that produces phycocyanobilin, a main chromophore for the CBCRs. We found that six of these CBCRs covalently bound a chromophore and exhibited variable properties, including blue/green, blue/teal, green/teal, and blue/orange reversible photoconversions. Notably, one CBCR, AM1_1870g4, displayed unidirectional photoconversion in response to blue light illumination, with a rapid dark reversion that was temperature dependent. Furthermore, the photoconversion took place without *Z/E*

isomerization. This observation indicated that AM1_1870g4 likely functions as a blue light power sensor, whereas typical CBCRs sense ratio of two light qualities. We also found that AM1_1870g4 possesses a GDCF motif in which the Asp residue is swapped with the next Gly residue within the DXCF motif. Site-directed mutagenesis revealed that this swap is essential for the light-power sensing function of AM1_1870g4. This is the first report of a blue-light power sensor from the CBCR superfamily and of photoperception without *Z/E* isomerization among the bilin-based photoreceptors.

INTRODUCTION

Photosynthetic organisms utilize light not only as an energy source but also as a signal. Linear tetrapyrrole (bilin) chromophores are involved in both of these functions, which involve the photosynthetic antenna complex, phycobilisomes, and photoreceptor families of phytochromes and cyanobacteriochromes (CBCRs). Phycobiliproteins covalently bind phycocyanobilin (PCB), phycoerythrobilin, phycoviolobilin (PVB), and phycourobilin to transfer the light energy to chlorophyll (1, 2). They stably absorb specific light qualities,

although phycoerythrocyanin shows unexpected photoconversion in vitro (3). Conversely, phytochromes and CBCRs covalently bind a linear tetrapyrrole chromophore and show reversible photoconversion that is triggered by *Z/E* isomerization of the double bond between the C and D rings (4, 5).

The phytochromes and CBCRs commonly possess a cGMP phosphodiesterase/adenylate cyclase/FhlA (GAF) domain that plays a central role in chromophore incorporation. Only the GAF domain is needed for proper photoconversion of the CBCRs, whereas N-terminal Per/Arnt/Sim (PAS) and/or phytochrome-specific (PHY) domains are also needed for proper photoconversion of the phytochromes (5). The light qualities sensed by the phytochromes are mostly restricted to the red-to-far-red region, although algal phytochromes show diverse spectral properties (6). Conversely, the light qualities sensed by CBCR GAF domains vary widely, ranging from ultraviolet to far-red. To date, biliverdin (BV), PCB, and PVB are known to bind to the CBCR apoprotein as a chromophore via a conserved canonical Cys residue (7–9). The CBCRs are categorized into various subfamilies and their color-tuning mechanisms are correspondingly diverse. Among them, two-Cys CBCRs have been detected from several distinct subfamilies (10–13). For most of these, the second Cys residue transiently ligates to C10 of the chromophore during the photoconversion cycle (10–16). Ligation of the second Cys residue to C10 results in a large blue-shift due to shortening of the conjugated system of the chromophore. Among the two-Cys CBCRs, DXCF CBCRs are widely distributed among cyanobacteria and are the most intensively analyzed so far (7, 10, 14, 17–32).

The DXCF CBCRs covalently bind PCB, catalyze isomerization from PCB to PVB in most cases, and sense a relatively short wavelength region from ultraviolet to orange (10, 17–19, 22, 23, 28, 30, 32). In addition to reversible covalent bond formation via the second Cys residue, the binding chromophore species and other color-tuning events determine the distinctive spectral properties of the DXCF CBCRs. Most of the DXCF CBCRs, including TePixJ and SesA, covalently bind PVB and show reversible

photoconversion between a blue-absorbing form (Pb) with 15*Z* PVB and a green-absorbing (Pg) form with 15*E* PVB (10, 17). PCB attachment resulted in a red-shifted orange-absorbing form (Po) with the 15*E* isomer that is free from the second Cys residue (25, 28). In the case of blue/teal-reversible CBCRs, the trapped twist model explains the blue-shifted teal-absorbing (Pt) states in which the D ring is highly twisted from the plane of the B-C rings, resulting in removal from the conjugated system (25, 27).

Recent studies have revealed that some CBCRs show very fast dark reversion from the 15*E* photoproduct to the 15*Z* dark state. Some red/green CBCRs show unidirectional photoconversion from a red-absorbing 15*Z* dark state to a green-absorbing 15*E* photoproduct and fast dark reversion from the 15*E* photoproduct to the 15*Z* dark state (33, 34). Recently identified DXCIP CBCRs that lack the canonical Cys residue but possess the DXCF Cys residue within the highly conserved DXCIP motif show unidirectional photoconversion from a 15*Z* dark state to a 15*E* photoproduct in response to green light illumination, and dark reversion from the 15*E* photoproduct to the 15*Z* dark state (35). In both cases, the equilibrium between the dark state and the photoproduct is set by two parameters: light intensity and temperature. A higher light intensity and/or lower temperature shift this equilibrium to favor of the photoproduct. In this regard, these photoreceptors can integrate light intensity and temperature signals. While red/green CBCRs and DXCIP CBCRs are responsive to red light intensity and green light intensity, respectively, no CBCRs responsive to blue light intensity have been described.

It recently has been reported that the chlorophyll *d*-bearing cyanobacterium *Acaryochloris marina* possesses various CBCRs with unique spectral properties. Red/blue and far-red/orange reversible photoconversions have been identified within the “expanded red/green” (XRG) CBCR lineage (9, 13, 36–38). The former photoconversion is based on PCB incorporation and reversible Cys attachment (13), while the latter photoconversion is established by BV incorporation (9, 36, 37).

In this study, we focused on the seven DXCF CBCRs from *A. marina*. We expressed

these CBCRs in PCB-producing *Escherichia coli* and analyzed their spectral properties. As a result, blue/green, blue/teal, green/teal, and blue/orange reversible photoconversions were identified. Interestingly, one of the DXCF CBCRs, AM1_1870g4, showed unidirectional photoconversion in response to blue light and fast dark reversion. This is the first report identifying a blue light power sensor from the CBCR superfamily.

RESULTS and DISCUSSION

DXCF-type CBCRs from A. marina

There are 82 GAF domains in 47 proteins coded by the *A. marina* genome. The GAF domain superfamily consists of many families, such as heme-binding, cyclic nucleotide-binding, and linear tetrapyrrole-binding families (39). In the case of *A. marina*, 2 domains for the cyclic nucleotide binding family (AM1_1841g1 and AM1_1841g2) and 24 domains for the linear tetrapyrrole-binding family were detected. Among these 24 domains, AM1_1870g1 and AM1_5894g were categorized into the phytochrome subfamily (Fig. 1). The other 22 GAF domains were categorized into the CBCR subfamily. Of these, 15 GAF domains retained the canonical Cys residue and so are likely to covalently bind the linear tetrapyrrole chromophore (Fig. 1). They were divided into the DXCF lineage (AM1_1378g, AM1_0048g1, AM1_0048g2, AM1_6305g1, AM1_0829g, AM1_1870g4, AM1_5997g4, AM1_5704g1 and AM1_1499g1), the XRG lineage (AM1_1557g2, AM1_C0023g2, AM1_1186g2, AM1_1870g3 and AM1_6305g2) and the FR/X lineage (AM1_5997g1). We previously analyzed the CBCR GAF domains of the XRG lineage and identified photochemical diversity (9, 13, 36, 37).

We focused on the GAF domains of the DXCF lineage because of their sequence variation (Fig. 1). AM1_5704g1 and AM1_1499g1 lack the second Cys residue within the DXCF motif. To address two-Cys photocycle in this study, we analyzed the other seven CBCR GAF domains (AM1_1378g, AM1_0048g1, AM1_0048g2, AM1_6305g1, AM1_0829g, AM1_1870g4, and AM1_5997g4) (Fig. 2A, domains highlighted by dotted squares). Among them, AM1_1870g4

possesses an arranged GDCF motif, in which the Asp residue is swapped with the next residue. These seven CBCR GAF domains also retain residues that are important for chromophore incorporation and proper photoconversion, including the canonical Cys residue (Fig. 2B).

In previous studies, by co-expressing heme oxygenase and PcyA to produce PCB in *E. coli*, the known GAF domains of the DXCF lineage were revealed to bind PCB and catalyze isomerization from PCB to PVB in some cases (14, 18, 28, 32). Based on these findings, we also expressed the seven GAF domains as His-tagged proteins in PCB-producing *E. coli* and purified them by nickel-affinity chromatography. All GAF domains except AM1_5997g4 are likely to covalently bind a linear tetrapyrrole chromophore, as judged by zinc-induced fluorescence detection (Fig. 3A). Further, denatured spectra corresponded well to the covalently bonded PCB or PVB, as described below (see Fig. 5 and Fig. 6B). We could not detect any mutations critical for chromophore binding in AM1_5997g4 based on sequence comparison (Fig. 2B). In the case of AM1_1378g, a major band in the CBB-stained gel did not correspond to a zinc-induced fluorescent band (Fig. 3A). Instead, a minor band in the CBB-stained gel (Fig. 3A, triangle) well corresponded to the fluorescent band. Together with a very low specific absorbance ratio (SAR) value (Table 2), this minor band in the CBB-stained gel was concluded to be AM1_1378g (Fig. 3A). In total, intensities of CBB-stained bands did not correspond well to those of zinc-induced fluorescent bands (Fig. 3A). This is due to two parameters; binding chromophore species and binding efficiency. By additionally taking the SAR values into consideration (Table 2), we concluded that the binding efficiencies of AM1_0048g1 and AM1_6305g1 were better than seen with the other CBCR GAF domains. Next, we performed spectral analyses using native and acid-denatured proteins. We describe these results for each photocycle type.

Blue/green photocycle: AM1_1378g

To assess the chromophore structures binding to the CBCR GAF domains, we used an acid denaturation assay. Since chemical

denaturation removes interactions with the protein, the absorbance spectra and photochemistry of denatured biliproteins can be used to identify their bilin chromophore species and to assign C15 double-bond configurations (3, 40). The 15*E* chromophores of urea-denatured biliproteins that absorb a shorter wavelength region can photoisomerize to 15*Z* and absorb a longer wavelength region, but 15*Z* chromophores are inert. Covalently bonded 15*Z*- and 15*E*-PCB showed absorption maxima around 660 nm and 600 nm, respectively, while covalently bonded 15*Z*- and 15*E*-PVB showed absorption maxima around 600 nm and 530 nm, respectively. In the case of a mixture of PCB and PVB, two absorbance peaks around 660 nm and 600 nm were detected for the 15*Z*-chromophores.

Based on the spectral properties of the native and acid-denatured proteins, AM1_1378g covalently bound PVB and showed reversible photoconversion between a Pb form with a 15*Z*-isomer peaking at 414 nm and a Pg form with a 15*E*-isomer peaking at 525 nm (Fig. 4A, Fig. 5A, Fig. 6, Table 2). Because PVB but not PCB was observed in the acid-denatured spectra (Fig. 5A and Fig. 6B), isomerization from PCB to PVB was quite efficient even in *E. coli*. AM1_1378 has an MA domain for signal-output and is orthologous to SyPixJ1 and TePixJ, the CBCR GAF domains of which also show blue/green reversible photoconversion (Fig. 2A) (17, 23)

Blue/teal photocycle: AM1_0048g1 and AM1_0048g2

Based on the spectral properties of the native and acid-denatured proteins, AM1_0048g1 covalently bound both PCB and PVB and showed reversible photoconversion between a Pb form with a 15*Z*-isomer peaking at 418 nm and a Pt form with a 15*E*-isomer peaking at 498 nm (Fig. 4B, Fig. 5B, Fig. 6, Table 2). Similarly, AM1_0048g2 covalently bound both PCB and PVB and showed reversible photoconversion between a Pb form with a 15*Z*-isomer peaking at 409 nm and a Pt form with a 15*E*-isomer peaking at 506 nm (Fig. 4C, Fig. 5C, Fig. 6, Table 2). A very low level of PCB corresponding to an absorbance around 662 nm for the denatured spectrum of the 15*Z*-isomer was detected for AM1_0048g1, whereas AM1_0048g2 bound a

larger amount of PCB corresponding to the same absorbance region (Fig. 5B, C). Difference spectra of the denatured proteins also support this interpretation (Fig. 6B). The absorption intensity around 605 nm was higher than that around 669 nm for AM1_0048g1 but lower for AM1_0048g2 (Fig. 6B). Because the conjugated system of PCB is extended to the ring A, PCB chromophorylation should result in a red shift of the native 15*E*-isomer whose chromophore is free from the second Cys residue. Notably, both Pt forms contained red-shifted absorption shoulders around 570 nm (Fig. 4B-C). Irradiation of the red-shifted components of AM1_0048g1 and AM1_0048g2 with orange and red light sources peaking at 590 nm and 650 nm, respectively, resulted in photoconversion to the Pb forms (Fig. 7, orange lines). The red-shifted shoulder absorption of AM1_0048g2 was more prominent than that of AM1_0048g1 (Figs. 4B, 4C), which is consistent with the finding that the binding ratio of PCB to PVB in AM1_0048g2 was higher than that in AM1_0048g1 (Figs. 5B, C, 6B). All these results demonstrate that the red-shifted components correspond to those that bind PCB. In both cases, the absorption peaks of the Pb forms of the PCB-binding components (Fig. 7, orange lines) are almost same as those that bind PVB (Fig. 7, blue lines). A mixture of PCB and PVB was also observed for the other CBCRs, when reconstituted in the PCB-producing *E. coli* (14, 18–20, 22, 28, 32). However, when the same CBCR GAF domains were expressed in the cyanobacterial cells, the binding chromophore consisted of only the PVB chromophore (7, 18–20, 22). Thus, AM1_0048g1 and AM1_0048g2 are also expected to bind only PVB in the cyanobacterial cells. Unknown factors may be needed for proper isomerization activity from PCB to PVB.

Some blue/teal-reversible CBCRs retain two Phe residues that are predicted to be located close to ring D, and these Phe residues have been shown to play a role in twisting ring D from the plane of the B-C rings to form blue-shifted Pt forms (27). As AM1_0048g1 also retains these two Phe residues, its Pt formation should be established by a similar mechanism; however, AM1_0048g2 does not possess these Phe residues, indicating involvement of other residues in Pt formation. Tlr1999 derived from

Thermosynechococcus elongatus BP-1 also showed a similar blue/teal-reversible photoconversion without these Phe residues (22).

AM1_0048 has two blue/teal-reversible CBCR GAF domains but no known signal-output domains. At its C-terminus region, however, there is a region consisting of approximately 300 amino acid residues with no known functional domains (Fig. 2A), indicating that this region may function in some sort of signaling role.

Green/teal photocycle: AM1_6305g1

Based on the spectral properties of the native and acid-denatured proteins, AM1_6305g1 covalently bound PVB and showed reversible photoconversion between the Pg form with a 15Z-isomer peaking at 557 nm and the Pt form with a 15E-isomer peaking at 491 nm (Fig. 4D, Fig. 5D, Fig. 6, Table 2). Because the Pt form of AM1_6305g1 is spectrally similar to those of blue/teal-reversible CBCRs, the Pt form of AM1_6305g1 is likely to be free from the second Cys residue as well as the other Pt forms (22, 25, 28). The chromophore of the Pg form is apparently free from the second Cys residue because of its red-shifted absorbance. Thus, the second Cys residue should not be covalently bound to the chromophore in either form. To verify this speculation, we added iodoacetamide (IAM) to both the Pg and Pt forms of AM1_6305g1 at a final concentration of 50 mM (Fig. 8), which is an excessive amount relative to the protein concentration and is sufficient to block Cys residues of the other CBCR GAF domains (13, 22). Protein samples were incubated for 30 min after IAM addition. In both cases, IAM addition had little effect on their spectral properties. In the presence of IAM, both Pt and Pg forms showed teal/green reversible photoconversion. These results demonstrate that the second Cys residue is not covalently bound to the chromophore in either form. Conversely, the acid-denatured spectra clearly showed that only the PVB chromophore attached to AM1_6305g1 (Fig. 5D). In AM1_6305g1, the second Cys residue did not contribute to covalent bond formation but rather to efficient isomerization from PCB to PVB.

In previous studies, two CBCRs, NpR5113g1 and DpxA from *Nostoc punctiforme*

and *Fremyella diplosiphon*, respectively, were reported to show green/teal-reversible photoconversion (28, 29). Interestingly, although NpR5113g1 and DpxA are definitely orthologous to each other, AM1_6305g1 is not a closely related ortholog of these two GAF domains (Fig. 1). NpR1597g1 and NpR5113g3, which show blue/teal reversible photoconversion, are phylogenetically closer to NpR5113g1 and DpxA than AM1_6305g1. Complicated evolutionary event(s) have likely occurred within this cluster. Although we tried to identify residues specifically conserved among these three green/teal-reversible CBCRs in comparison with other blue/teal DXCF CBCRs (22, 28, 29, 32), we could not identify such residues near the chromophore based on the structure. Thus, multiple residues may indirectly affect positioning of the second Cys to interfere with covalent bond formation in their Pg forms.

Blue/orange photocycle: AM1_0829g

Based on the spectral properties of the native and acid-denatured proteins, AM1_0829g covalently bound PCB and showed reversible photoconversion between the Pb form with a 15Z-isomer peaking at 417 nm and the Po form with a 15E-isomer peaking at 579 nm (Fig. 4E, Fig. 5E, Fig. 6, Table 2). No PVB chromophore was detected from the acid-denatured spectra (Fig. 5E), indicating no isomerization activity from PCB to PVB. The Po form is red shifted in comparison with the Pg forms of the typical DXCF CBCRs. This red-shifted spectrum is due to PCB attachment in which the second Cys residue is free from the chromophore and so the conjugated system is extended to ring A to absorb orange light.

Some CBCRs that show blue/orange reversible photoconversion have previously been identified. These CBCRs are categorized into two subfamilies (Fig. 1, blue/orange and CikA subfamilies). One subfamily, which includes NpF4973, is characterized by a whole protein architecture being composed of only a GAF domain (26). Another subfamily contains CikA homologs, including SyCikA and NpF1000 (21, 28). Interestingly, AM1_0829g showed low sequence similarity with both subfamily CBCRs. In this context, AM1_0829g independently lost isomerization activity from PCB to PVB to sense

red-shifted orange light.

Blue/blue photocycle: AM1_1870g4.

Purified AM1_1870g4 absorbs blue light with an absorbance maximum at 416 nm (Fig. 9A, Table 2). We could not detect any photoconversion after blue light illumination. Therefore, we next measured the absorption spectrum during irradiation with blue light, taking the possibility of rapid dark reversion into consideration. As a result, irradiation of AM1_1870g4 with blue light resulted in a slight absorption increase (Fig. 9A). These measurements showed that the photoproduct state of AM1_1870g4 also absorbs blue light but is slightly red shifted relative to the dark-adapted form, with a maximum at 424 nm (Table 2). The spectral overlap of the dark-adapted form and the photoproduct results in a dark-minus-light difference spectrum with a maximum at 374 nm and a minimum at 437 nm (Fig. 9B), shifted relative to the observed peak wavelengths.

The rapid dark reversion observed with AM1_1870g4 raised the possibility that it might function as a sensor for light intensity, as reported for some red/green CBCRs and DXCIP CBCRs (33–35). To behave as a sensor for light intensity, dark reversion should be rapid enough that photoconversion of the photoproduct does not substantially contribute to photoequilibrium as well as the known light power sensors. Therefore, we monitored changes in absorbance at 424 nm during photoconversion and dark-reversion cycles with different light intensities at different temperatures (Fig. 10A). At all temperatures tested (15, 20, 25, and 30°C), the light-dependent absorbance changes decreased with lower light intensities. Plotting the change in absorbance at 424 nm (ΔA_{424}) versus light intensity demonstrated that ΔA_{424} increased and was almost, but not completely, saturated at 15°C, probably due to quite fast dark reversion (Fig. 10B). These results suggest that suppression of dark reversion at lower temperatures resulted in a shift of the equilibrium in favor of the light-adapted form.

We therefore measured dark-reversion kinetics at different temperatures. At all temperatures tested (15, 20, 25, and 30°C), semi-logarithmic plots of the dark-reversion kinetics were linear, indicating that dark reversion

is a first-order reaction (Fig. 10C). Slower dark reversion was observed at lower temperatures. These results are consistent with the results of the light intensity dependence described above. The half-lives at 15, 20, 25, and 30°C were 24.6, 12.0, 5.2, and 2.6 sec, respectively. An Arrhenius plot of the corresponding rate constants was constructed (Fig. 10D) and AM1_1870g4 exhibited a linear Arrhenius relationship. From this plot, we calculated the activation energy to be 26 kcal/mol. This value is higher than those (14–16 kcal/mol) of the light intensity sensors previously reported for the other CBCR lineage (33, 35). The higher activation energy means that AM1_1870g4 possesses higher thermosensitivity than the other light intensity sensors. Because the optimal temperature for growth of *A. marina* is around 25°C, AM1_1870g4 is likely to integrate light intensity and temperature signals in natural environments. A dark reversion property generally enables photoreceptors to sense light intensity signals in a temperature-dependent manner. In fact, other photoreceptors belonging to different families such as phytochrome, light, oxygen, or voltage (LOV) and blue-light using flavin (BLUF) proteins have also been revealed to show similar behaviors (41–45). In the case of the phytochrome proteins, Cph1 and Agp1 showed unexpected temperature-dependent His kinase activities, which affected conjugation in *Agrobacterium*. In this context, we should monitor output activity of the C-terminal His kinase activity under various light and temperature conditions to understand the detailed mechanisms integrating light intensity and temperature signals (46–48).

We next measured the acid-denatured spectra of both the dark-adapted form and the photoproduct (Fig. 11). To get as much photoproduct as possible, the sample was irradiated with strong blue light ($1320 \mu\text{mol m}^{-2} \text{s}^{-1}$) on ice prior to denaturation. As a result, both the dark-adapted form and photoproduct showed similar spectra peaking at 580 nm with a significant shoulder around 520 nm. In both cases, white light illumination resulted in a red shift and the final products corresponded well to covalently bound 15Z-PVB (Fig. 11A, B). These results mean that both forms contained 15Z- and 15E-PVB (Fig. 11). The photoproduct contained a slightly larger amount of the 15E-isomer than the

dark-adapted form (Fig. 11C). The photoproduct was produced by blue light illumination with $1320 \mu\text{mol m}^{-2} \text{s}^{-1}$ light intensity on ice. Under these conditions, photoconversion should be almost saturated, judging by the light-dependent absorbance change (Fig. 10A, B). In this context, the slightly larger amount of the 15*E*-isomer in the photoproduct is not likely to be derived from photoconversion of the native protein. Alternatively, this situation may be derived from photochemical equilibrium irrespective of photoconversion of the native protein. This hypothesis was also supported by a site-directed mutagenesis study, as described below.

If this hypothesis is correct, this protein may be the first example among the bilin-based photoreceptors that shows photoconversion without *Z/E* isomerization. Because AM1_1870g4 is present within the tandemly arranged GAF domain cluster (Fig. 2A), one may assume that AM1_1870g4 acts not as photoreceptor but as an antenna to transfer light energy to the other GAF domains. To verify such a possibility, we determined the fluorescence quantum yield of AM1_1870g4, which was calculated to be only 0.6%. This result clearly rejects the antenna role of AM1_1870g4. In order to further prove this hypothesis, it will be necessary to perform other experiments such as observation of light-dependent output activity. However, the current study may provide a clue for novel photoreceptors that bind phycoerythrobilin and phycourobilin, which contain no double bonds between the C and D rings.

Site-directed mutagenesis of AM1_1870g4.

AM1_1870g4 possesses a GDCF motif in which the Asp residue is swapped with the next residue in comparison with the canonical DXCF motif. This unique arrangement of the Asp position may be responsible for the blue light power sensing function. To test this, we swapped this motif back to the canonical DGCF motif. The mutant protein, AM1_1870g4-DGCF, efficiently incorporated PVB as well as the wild-type protein, and absorbed light in the blue region (Fig. 3B, Fig. 12A). AM1_1870g4-DGCF showed reversible photoconversion that is clearly distinct from that of the wild type protein (Fig. 12). The ground state with 15*Z*-PVB peaking at 420 nm (Fig. 12A

blue line, Fig. 13A) partially converted to the photoproduct with 15*E*-PVB peaking at 425 nm (Fig. 12A orange line, Fig. 13B). The ground state was generated upon irradiation with light around 470 nm, whereas the photoproduct was generated upon irradiation with light around 410 nm. Highly overlapped absorption spectra of these two states resulted in partial photoconversion. Reversible photoconversion was repeated without noticeable deterioration. The difference spectrum had a positive peak at 405 nm and a negative peak at 457 nm (Fig. 12B). These results indicate that the power sensing function without photoisomerization, as observed for the wild type protein, largely depend on the arranged “GDCF” motif. Blue light absorption of both forms suggests that the second Cys residue stably binds to the C10 of the chromophore. We introduced further mutations into AM1_1870g4-DGCF to try to obtain proteins showing typical blue/green reversible photoconversion based on sequence comparison, but have failed to do so to date (data not shown).

We next performed site-directed mutagenesis focused on the canonical Cys (C_{782}) and second Cys (C_{754}) residues (Fig. 14, 15). Singly ($C_{754}\text{S}$, $C_{782}\text{S}$) and doubly ($C_{754}\text{S}/C_{782}\text{S}$) mutated proteins were constructed. All variant proteins bound a chromophore, although $C_{782}\text{S}$ and $C_{754}\text{S}/C_{782}\text{S}$ variants exhibited reduced chromophore binding judging by the SAR values (Fig. 14, Table 2). Furthermore, these two variants ($C_{782}\text{S}$ and $C_{754}\text{S}/C_{782}\text{S}$) showed no covalent bond formation as assessed by fluorescence detection (Fig. 3C). The canonical Cys residue, C_{782} , was essential for covalent bonding and efficient chromophore incorporation, while the $C_{754}\text{S}$ variant efficiently incorporated the chromophore comparable with the wild-type protein (Fig. 3C). None of these variants showed any detectable photoconversion or dark reversion (Fig. 14), indicating that these Cys residues are essential for the light power sensing function of AM1_1870g4. Both $C_{754}\text{S}$ and $C_{754}\text{S}/C_{782}\text{S}$ variants, which lack the second Cys residue, absorbed light in the red region (Fig. 14A, 14C), probably due to no isomerization from PCB to PVB and no covalent bond formation between the second Cys residue and C10 of the chromophore. However, the $C_{782}\text{S}$ variant absorbed light in the blue region (Fig.

14B), probably due to covalent bond formation between the second Cys residue and C10 of the chromophore. Acid urea denaturation revealed that no variants bound any PVB chromophore species (Fig. 15). Not only the second Cys residue but also the canonical Cys residue is essential for isomerization activity from PCB to PVB. Denatured C₇₈₂S had a spectrum peaking around 600 nm with a significant shoulder around 700 nm, and white light illumination after denaturation resulted in a red shift peaking around 700 nm (Fig. 15B). These results suggest that the chromophores of the C₇₈₂S variant are a mixture of the 15Z-isomer and the 15E-isomer, which is similar to the wild-type protein. However, white light illumination after denaturation did not affect the absorption spectra of the C₇₅₄S and C₇₅₄S/C₇₈₂S variants (Fig. 15A, 15C), indicating that their bound chromophores consisted of only 15Z-isomers. Together with the DGCF mutation analysis, covalent bond formation between the second Cys residue (C₇₅₄) and C10 and the arranged “GDGF” motif may result in accumulation of the 15E-isomer to some extent, irrespective of photoconversion. The denatured spectrum of the C₇₅₄S variant peaking at 665 nm corresponds to that of covalently bound 15Z-PCB (Fig. 15A). Conversely, the 15Z-isomers of the C₇₈₂S and C₇₅₄S/C₇₈₂S variants peaking at 676 and 689 nm, respectively, were red shifted in comparison with the covalently bound 15Z-PCB (Fig. 15B, 15C). Because these variants lack the canonical Cys residue, these red-shifted components should correspond to non-covalently bound 15Z-PCB. In line with this assumption, the photochemical difference spectrum of the denatured C₇₈₂S variant was red shifted in comparison with that of the covalently bound PCB (Fig. 15D).

Unique properties of AM1_1870.

AM1_1870 possesses a quite complicated domain architecture consisting of one phytochrome-type GAF domain and two CBCR GAF domains for light sensory input and two-component hybrid signaling systems for output (Fig. 2A) (36). To characterize the phytochrome-type GAF domain of AM1_1870, we expressed AM1_1870g1-g2 covering the GAF-PHY region (Fig. 2A) in the PCB-producing

E. coli. Although the purified fraction included many contaminating proteins, probably due to low expression yield, zinc-induced fluorescence was detected from the protein band at approximately 60 kDa (Fig. 16 inset, arrowheads), which corresponds well to the theoretical molecular weight. The purified AM1_1870g1-g2 could bind PCB and showed red/far-red reversible photoconversion (Fig. 16). Together with a previous study (36), AM1_1870 is concluded to possess three light sensory systems: red/far-red, blue/blue and red/green sensing systems.

There have been no reports of CBCRs that sense blue light power. To date, red and green light power sensors have been identified (33–35). Most cyanobacteria possess flavin-binding photoreceptors such as LOV and BLUF proteins. Because flavin absorbs in the UV-to-blue region, they function as blue light sensors. Because some LOV and BLUF proteins derived from cyanobacteria show rapid dark reversion, they are also likely to function as a blue light power sensor (49, 50). Notably, BLUF proteins were not detected in *A. marina* genomic information. Although one LOV protein was detected in *A. marina*, this protein possesses an arranged SCHFL motif instead of the highly conserved NCRFL motif that is important for photoconversion. Although there is no experimental evidence, AM1_1870g4 may function as a blue light power sensor to compensate for a lack of flavin-based power sensors.

Recently, plant photoreceptors of phototropin and phytochrome B have been reported to integrate light and temperature signals *in vivo* (42–44). Because several CBCRs, including AM1_1870g4, integrate light and temperature signals *in vitro*, these photoreceptors are also likely to physiologically perceive both light and temperature signals *in vivo*. Future physiological studies in this regard are required.

Concluding remarks

In this study, we identified DXCF CBCR GAF domains showing blue/green, blue/teal, green/teal, blue/orange or blue/blue reversible photoconversion from *A. marina*. Together with previous studies of XRG CBCR GAF domains and a phytochrome protein from *A. marina* (9, 13, 36, 37, 51), *A. marina* can sense

various light qualities covering the blue-to-far-red wavelength range. It is of note that expression of only the GAF domain may not reflect the original spectral property of its full-length protein. In fact, phytochromes need the PAS and/or PHY domains in addition to the GAF domain for proper chromophore incorporation and photoconversion (52–54). Further studies such as spectral analyses using full-length proteins and physiological analyses using photoreceptor disruptants are needed to reveal detailed photoperception mechanisms.

EXPERIMENTAL PROCEDURES

Bacterial strains and growth media

The *Escherichia coli* strain JM109 was used for plasmid construction and the *E. coli* strain C41 harboring pKT271 that encodes heme oxygenase and PcyA to produce PCB, was used for protein expression (55). Bacterial cells were grown in Luria-Bertani (LB) medium containing kanamycin with or without chloramphenicol at 20 $\mu\text{g ml}^{-1}$. For protein expression, the cells were grown in LB medium at 37°C until the optical density at 600 nm was 0.4–0.8 and then isopropyl β -D-1-thiogalactopyranoside (IPTG) was added at a final concentration of 0.1 mM. Subsequently, the cells were cultured at 18°C overnight followed by collection of the cell pellets by centrifugation.

Bioinformatics

Nucleotide and amino acid sequences of DXCF CBCR proteins from *A. marina* were obtained from CyanoBase (56). Motif analyses were performed by SMART searches run on the internet (57). Multiple sequence alignments were constructed using CLUSTAL_X and manually edited based on the structural information of TePixJ (58). The phylogenetic tree was constructed by the neighbor-joining method and visualized by using iTOL on the internet (59).

Plasmid construction

DXCF CBCR GAF domains were amplified from *A. marina* genomic DNA using PrimeSTAR Max DNA polymerase and the appropriate nucleotide primers (Table 1). The amplified DNA fragments were cloned into the plasmid pET28a and site-directed mutagenesis was performed as previously described using appropriate primers

(35) (Table 1). All expression constructs were verified by nucleotide sequencing.

Protein expression and purification

The His-tagged proteins were expressed in *E. coli* C41 pKT271. Cells were disrupted in buffer A (20 mM HEPES-NaOH, pH 7.5, 0.1 M NaCl, and 10 % (w/v) glycerol) containing 0.5 mM Tris(2-carboxyethyl)phosphine (TCEP) by three passages through an Emulsiflex C5 high-pressure homogenizer at 83 MPa (Avestin). The mixture was centrifuged at 165,000 $\times g$ for 30 min, and then the supernatants were loaded onto a nickel-affinity His-trap column (GE Healthcare) using the ÄKTAprime plus chromatography system (GE Healthcare) after filtration with a 0.2 μm cellulose ether membrane. The column was washed with buffer A containing 100 mM imidazole, and then the His-tagged proteins were eluted with a linear gradient of buffer A containing 100–400 mM imidazole. Following incubation with 1 mM EDTA for 1 h, the proteins were dialyzed against buffer A containing 1 mM dithiothreitol (DTT) without EDTA and imidazole.

Electrophoresis and zinc-induced fluorescence assay

Purified proteins in 2% (w/v) sodium dodecyl sulfate (SDS), 60 mM DTT, and 60 mM Tris-HCl (pH 8.0) were separated using SDS polyacrylamide gel electrophoresis (PAGE) with a 12% (w/v) acrylamide gel, followed by staining with Coomassie Brilliant Blue R-250 (CBB). For the zinc-induced fluorescence assay after SDS-PAGE, the gel was soaked in 20 mM zinc acetate at room temperature for 30 min. Fluorescence was then visualized through a 600-nm long-path filter upon excitation with blue ($\lambda_{\text{max}} = 470 \text{ nm}$), and green ($\lambda_{\text{max}} = 527 \text{ nm}$) light through a 562 nm short-path filter using WSE-6100 LuminoGraph (ATTO) and WSE-5500 VariRays (ATTO) machines.

Spectroscopy and dark-reversion kinetics

Ultraviolet and visible absorption spectra of the proteins were recorded with a UV-2600 spectrophotometer (SHIMADZU) at 15, 20, 25, and 30°C using a temperature controller. Monochromatic light of various wavelengths for

photoconversion was generated using an Opto-Spectrum Generator (Hamamatsu Photonics, Inc.). Acid denaturation used 8 M urea, pH 2.0, followed by recording an absorption spectrum, white light illumination for 3 min, and recording of a second absorption spectrum.

To monitor the photoconversion and dark-reversion processes, absorbance at 424 nm of the proteins against various intensities of blue

light (430 nm; 1320, 1130, 1020, 890, 750, 620, 490, 360, 230, 90, 30, 15 and 5 $\mu\text{mol m}^{-2} \text{s}^{-1}$) was measured for 15 s with dark intervals of 90 s. The half-lives and the Arrhenius parameters were estimated from the dark-reversion kinetics at the different temperatures. The fluorescence quantum yield was measured with Quantaaurus-QY (Hamamatsu Photonics, Inc.).

ACKNOWLEDGMENTS

This work was supported by JST, CREST (JPMJCR1653 to R.N.), and JSPS KAKENHI (26702036 to R.N.). The authors would like to thank Enago (www.enago.jp) for the English language review.

CONFLICT OF INTEREST

The authors declare that they have no conflicts of interest with the contents of this article

AUTHOR CONTRIBUTIONS

M.H. and R.N. designed the research. M.H., K.F., K.M. and Y.O. prepared plasmids for protein expression. M.H., K.F., K.M. and T.N. purified proteins and performed spectroscopic analyses. M.H., K.F., T.N., G.E., M.S., M.I. and R.N. analyzed the data. M.H. and R.N. wrote the manuscript.

REFERENCES

1. Singh, N. K., Sonani, R. R., Rastogi, R. P., and Madamwar, D. (2015) The phycobilisomes: an early requisite for efficient photosynthesis in cyanobacteria. *EXCLI J.* **14**, 268–89
2. Watanabe, M., and Ikeuchi, M. (2013) Phycobilisome: architecture of a light-harvesting supercomplex. *Photosyn. Res.* **116**, 265–76
3. Zhao, K.-H., Haessner, R., Cmiel, E., and Scheer, H. (1995) Type I reversible photochemistry of phycoerythrocyanin involves *Z/E*-isomerization of -84 phycoviolobin chromophore. *Biochim. Biophys. Acta* **1228**, 235–243
4. Anders, K., and Essen, L.-O. O. (2015) The family of phytochrome-like photoreceptors: diverse, complex and multi-colored, but very useful. *Curr. Opin. Struct. Biol.* **35**, 7–16
5. Ikeuchi, M., and Ishizuka, T. (2008) Cyanobacteriochromes: a new superfamily of tetrapyrrole-binding photoreceptors in cyanobacteria. *Photochem. Photobiol. Sci.* **7**, 1159–1167
6. Rockwell, N. C., Duanmu, D., Martin, S. S., Bachy, C., Price, D. C., Bhattacharya, D., Worden, A. Z., and Lagarias, J. C. (2014) Eukaryotic algal phytochromes span the visible spectrum. *Proc. Natl. Acad. Sci. U.S.A.* **111**, 3871–3876
7. Ishizuka, T., Narikawa, R., Kohchi, T., Katayama, M., and Ikeuchi, M. (2007) Cyanobacteriochrome TePixJ of *Thermosynechococcus elongatus* harbors phycoviolobin as a chromophore. *Plant Cell Physiol.* **48**, 1385–1390
8. Narikawa, R., Fukushima, Y., Ishizuka, T., Itoh, S., and Ikeuchi, M. (2008) A novel photoactive GAF domain of cyanobacteriochrome AnPixJ that shows reversible green/red photoconversion. *J. Mol. Biol.* **380**, 844–855
9. Narikawa, R., Nakajima, T., Aono, Y., Fushimi, K., Enomoto, G., Ni-Ni-Win, Itoh, S., Sato, M., and Ikeuchi, M. (2015) A biliverdin-binding cyanobacteriochrome from the chlorophyll *d*-bearing cyanobacterium *Acaryochloris marina*. *Sci. Rep.* **5**, 7950
10. Rockwell, N. C., Njuguna, S. L., Roberts, L., Castillo, E., Parson, V. L., Dwojak, S., Lagarias, J. C., and Spiller, S. C. (2008) A second conserved GAF domain cysteine is required for the blue/green photoreversibility of cyanobacteriochrome Tlr0924 from *Thermosynechococcus elongatus*. *Biochemistry* **47**, 7304–7316

11. Rockwell, N. C., Martin, S. S., and Lagarias, J. C. (2017) There and back again: Loss and reacquisition of two-Cys photocycles in cyanobacteriochromes. *Photochem. Photobiol.* **93**, 741–754
12. Rockwell, N. C., Martin, S. S., Feoktistova, K., and Lagarias, J. C. (2011) Diverse two-cysteine photocycles in phytochromes and cyanobacteriochromes. *Proc. Natl. Acad. Sci. U.S.A.* **108**, 11854–11859
13. Narikawa, R., Enomoto, G., Ni-Ni-Win, Fushimi, K., and Ikeuchi, M. (2014) A new type of dual-Cys cyanobacteriochrome GAF domain found in cyanobacterium *Acaryochloris marina*, which has an unusual red/blue reversible photoconversion cycle. *Biochemistry* **53**, 5051–5059
14. Ishizuka, T., Kamiya, A., Suzuki, H., Narikawa, R., Noguchi, T., Kohchi, T., Inomata, K., and Ikeuchi, M. (2011) The cyanobacteriochrome, TePixJ, isomerizes its own chromophore by converting phycocyanobilin to phycoviolobilin. *Biochemistry* **50**, 953–961
15. Narikawa, R., Ishizuka, T., Muraki, N., Shiba, T., Kurisu, G., and Ikeuchi, M. (2013) Structures of cyanobacteriochromes from phototaxis regulators AnPixJ and TePixJ reveal general and specific photoconversion mechanism. *Proc. Natl. Acad. Sci. U.S.A.* **110**, 918–923
16. Burgie, E. S., Walker, J. M., Phillips, G. N., and Vierstra, R. D. (2013) A photo-labile thioether linkage to phycoviolobilin provides the foundation for the blue/green photocycles in DXCF-cyanobacteriochromes. *Structure* **21**, 88–97
17. Ishizuka, T., Shimada, T., Okajima, K., Yoshihara, S., Ochiai, Y., Katayama, M., and Ikeuchi, M. (2006) Characterization of cyanobacteriochrome TePixJ from a thermophilic cyanobacterium *Thermosynechococcus elongatus* strain BP-1. *Plant Cell Physiol.* **47**, 1251–1261
18. Narikawa, R., Suzuki, F., Yoshihara, S., Higashi, S., Watanabe, M., and Ikeuchi, M. (2011) Novel photosensory two-component system (PixA-NixB-NixC) involved in the regulation of positive and negative phototaxis of cyanobacterium *Synechocystis* sp. PCC 6803. *Plant Cell Physiol.* **52**, 2214–2224
19. Enomoto, G., Ni-Ni-Win, Narikawa, R., and Ikeuchi, M. (2015) Three cyanobacteriochromes work together to form a light color-sensitive input system for c-di-GMP signaling of cell aggregation. *Proc. Natl. Acad. Sci. U.S.A.* **112**, 8082–8087
20. Enomoto, G., Nomura, R., Shimada, T., Ni-Ni-Win, Narikawa, R., and Ikeuchi, M. (2014) Cyanobacteriochrome SesA is a diguanylate cyclase that induces cell aggregation in *Thermosynechococcus*. *J. Biol. Chem.* **289**, 24801–24809
21. Narikawa, R., Kohchi, T., and Ikeuchi, M. (2008) Characterization of the photoactive GAF domain of the CikA homolog (SyCikA, Slr1969) of the cyanobacterium *Synechocystis* sp. PCC 6803. *Photochem. Photobiol. Sci.* **7**, 1253–1259
22. Enomoto, G., Hirose, Y., Narikawa, R., and Ikeuchi, M. (2012) Thiol-based photocycle of the blue and teal light-sensing cyanobacteriochrome Tlr1999. *Biochemistry* **51**, 3050–3058
23. Yoshihara, S., Katayama, M., Geng, X., and Ikeuchi, M. (2004) Cyanobacterial phytochrome-like PixJ1 holoprotein shows novel reversible photoconversion between blue- and green-absorbing forms. *Plant Cell Physiol.* **45**, 1729–1737
24. Yoshihara, S., Shimada, T., Matsuoka, D., Zikihara, K., Kohchi, T., and Tokutomi, S. (2006) Reconstitution of blue-green reversible photoconversion of a cyanobacterial photoreceptor, PixJ1, in phycocyanobilin-producing *Escherichia coli*. *Biochemistry* **45**, 3775–84
25. Rockwell, N. C., Martin, S. S., and Lagarias, J. C. (2012) Mechanistic insight into the photosensory versatility of DXCF cyanobacteriochromes. *Biochemistry* **51**, 3576–3585
26. Rockwell, N. C., Martin, S. S., and Lagarias, J. C. (2015) Identification of DXCF cyanobacteriochrome lineages with predictable photocycles. *Photochem. Photobiol. Sci.* **14**, 929–941
27. Rockwell, N. C., Martin, S. S., Gulevich, A. G., and Lagarias, J. C. (2014) Conserved phenylalanine residues are required for blue-shifting of cyanobacteriochrome photoproducts. *Biochemistry* **53**, 3118–3130
28. Rockwell, N. C., Martin, S. S., Gulevich, A. G., and Lagarias, J. C. (2012) Phycoviolobilin formation and spectral tuning in the DXCF cyanobacteriochrome subfamily. *Biochemistry* **51**, 1449–1463

29. Wiltbank, L. B., and Kehoe, D. M. (2016) Two cyanobacterial photoreceptors regulate photosynthetic light harvesting by sensing teal, green, yellow, and red light. *MBio* **7**, e02130–15
30. Cho, S. M., Jeoung, S. C., Song, J.-Y. Y., Kupriyanova, E. V., Pronina, N. A., Lee, B.-W. W., Jo, S.-W. W., Park, B.-S. S., Choi, S.-B. B., Song, J.-J. J., and Park, Y.-I. I. (2015) Genomic survey and biochemical analysis of recombinant candidate cyanobacteriochromes reveals enrichment for near UV/violet sensors in the halotolerant and alkaliphilic cyanobacterium *Microcoleus* IPPAS B353. *J. Biol. Chem.* **290**, 28502–28514
31. Song, J.-Y. Y., Cho, H. S., Cho, J.-I. I., Jeon, J.-S. S., Lagarias, J. C., and Park, Y.-I. I. (2011) Near-UV cyanobacteriochrome signaling system elicits negative phototaxis in the cyanobacterium *Synechocystis* sp. PCC 6803. *Proc. Natl. Acad. Sci. U.S.A.* **108**, 10780–10785
32. Ma, Q., Hua, H.-H. H., Chen, Y., Liu, B.-B. B., Krämer, A. L., Scheer, H., Zhao, K.-H. H., and Zhou, M. (2012) A rising tide of blue-absorbing biliprotein photoreceptors: characterization of seven such bilin-binding GAF domains in *Nostoc* sp. PCC7120. *FEBS J.* **279**, 4095–108
33. Fushimi, K., Enomoto, G., Ikeuchi, M., and Narikawa, R. (2017) Distinctive properties of dark reversion kinetics between two red/green-type cyanobacteriochromes and their application in the photoregulation of cAMP synthesis. *Photochem. Photobiol.* **93**, 681–691
34. Rockwell, N. C., Martin, S. S., and Lagarias, J. C. (2012) Red/green cyanobacteriochromes: sensors of color and power. *Biochemistry* **51**, 9667–9677
35. Fushimi, K., Rockwell, N. C., Enomoto, G., Ni-Ni-Win, Martin, S. S., Gan, F., Bryant, D. A., Ikeuchi, M., Lagarias, J. C., and Narikawa, R. (2016) Cyanobacteriochrome photoreceptors lacking the canonical Cys residue. *Biochemistry* **55**, 6981–6995
36. Narikawa, R., Fushimi, K., Ni-Ni-Win, and Ikeuchi, M. (2015) Red-shifted red/green-type cyanobacteriochrome AM1_1870g3 from the chlorophyll *d*-bearing cyanobacterium *Acaryochloris marina*. *Biochem. Biophys. Res. Commun.* **461**, 390–395
37. Fushimi, K., Nakajima, T., Aono, Y., Yamamoto, T., Ni-Ni-Win, Ikeuchi, M., Sato, M., and Narikawa, R. (2016) Photoconversion and fluorescence properties of a red/green-type cyanobacteriochrome AM1_C0023g2 that binds not only phycocyanobilin but also biliverdin. *Front. Microbiol.* **7**, 588
38. Fushimi, K., Ikeuchi, M., and Narikawa, R. (2017) The expanded red/green cyanobacteriochrome lineage: An evolutionary hot spot. *Photochem. Photobiol.* **93**, 903–906
39. Aravind, L., and Ponting, C. P. (1997) The GAF domain: an evolutionary link between diverse phototransducing proteins. *Trends Biochem. Sci.* **22**, 458–9
40. Grombein, S., Rüdiger, W., and Zimmermann, H. (1975) The structures of the phytochrome chromophore in both photoreversible forms. *Hoppe-Seyler's Z. Physiol. Chem.* **356**, 1709–14
41. Abatedaga, I., Valle, L., Golic, A. E. E., Müller, G. L., Cabruja, M., Morán Vieyra, F. E., Jaime, P. C., Mussi, M. A. A., and Borsarelli, C. D. (2017) Integration of temperature and blue-light sensing in *Acinetobacter baumannii* through the BlsA sensor. *Photochem. Photobiol.* **93**, 805–814
42. Fujii, Y., Tanaka, H., Konno, N., Ogasawara, Y., Hamashima, N., Tamura, S., Hasegawa, S., Hayasaki, Y., Okajima, K., and Kodama, Y. (2017) Phototropin perceives temperature based on the lifetime of its photoactivated state. *Proc. Natl. Acad. Sci. U.S.A.* **114**, 9206–9211
43. Legris, M., Klose, C., Burgie, E. S., Rojas, C. C., Neme, M., Hiltbrunner, A., Wigge, P. A., Schäfer, E., Vierstra, R. D., and Casal, J. J. (2016) Phytochrome B integrates light and temperature signals in *Arabidopsis*. *Science* **354**, 897–900
44. Jung, J.-H. H., Domijan, M., Klose, C., Biswas, S., Ezer, D., Gao, M., Khattak, A. K., Box, M. S., Charoensawan, V., Cortijo, S., Kumar, M., Grant, A., Locke, J. C., Schäfer, E., Jaeger, K. E., and Wigge, P. A. (2016) Phytochromes function as thermosensors in *Arabidopsis*. *Science* **354**, 886–889
45. Burgie, E. S., Bussell, A. N., Lye, S.-H. H., Wang, T., Hu, W., McLoughlin, K. E., Weber, E. L., Li, H., and Vierstra, R. D. (2017) Photosensing and thermosensing by phytochrome B require both proximal and distal allosteric features within the dimeric photoreceptor. *Sci. Rep.* **7**, 13648

46. Njimonu, I., and Lamparter, T. (2011) Temperature effects on *Agrobacterium* phytochrome Agp1. *PLoS ONE* **6**, e25977
47. Njimonu, I., Yang, R., and Lamparter, T. (2014) Temperature effects on bacterial phytochrome. *PLoS ONE* **9**, e109794
48. Bai, Y., Rottwinkel, G., Feng, J., Liu, Y., and Lamparter, T. (2016) Bacteriophytochromes control conjugation in *Agrobacterium fabrum*. *J. Photochem. Photobiol. B, Biol.* **161**, 192–9
49. Narikawa, R., Zikihara, K., Okajima, K., Ochiai, Y., Katayama, M., Shichida, Y., Tokutomi, S., and Ikeuchi, M. (2006) Three putative photosensory light, oxygen or voltage (LOV) domains with distinct biochemical properties from the filamentous cyanobacterium *Anabaena* sp. PCC 7120. *Photochem. Photobiol.* **82**, 1627–33
50. Okajima, K., Yoshihara, S., Fukushima, Y., Geng, X., Katayama, M., Higashi, S., Watanabe, M., Sato, S., Tabata, S., Shibata, Y., Itoh, S., and Ikeuchi, M. (2005) Biochemical and functional characterization of BLUF-type flavin-binding proteins of two species of cyanobacteria. *J. Biochem.* **137**, 741–50
51. Loughlin, P. C., Duxbury, Z., Mugerwa, T. T., Smith, P. M., Willows, R. D., and Chen, M. (2016) Spectral properties of bacteriophytochrome AM1_5894 in the chlorophyll *d*-containing cyanobacterium *Acaryochloris marina*. *Sci. Rep.* **6**, 27547
52. Karniol, B., Wagner, J. R., Walker, J. M., and Vierstra, R. D. (2005) Phylogenetic analysis of the phytochrome superfamily reveals distinct microbial subfamilies of photoreceptors. *Biochem. J.* **392**, 103–16
53. Lamparter, T., Michael, N., Mittmann, F., and Esteban, B. (2002) Phytochrome from *Agrobacterium tumefaciens* has unusual spectral properties and reveals an N-terminal chromophore attachment site. *Proc. Natl. Acad. Sci. U.S.A.* **99**, 11628–33
54. Oka, Y., Matsushita, T., Mochizuki, N., Suzuki, T., Tokutomi, S., and Nagatani, A. (2004) Functional analysis of a 450-amino acid N-terminal fragment of phytochrome B in *Arabidopsis*. *Plant Cell* **16**, 2104–16
55. Mukougawa, K., Kanamoto, H., Kobayashi, T., Yokota, A., and Kohchi, T. (2006) Metabolic engineering to produce phytochromes with phytochromobilin, phycocyanobilin, or phycoerythrobilin chromophore in *Escherichia coli*. *FEBS Lett.* **580**, 1333–8
56. Fujisawa, T., Narikawa, R., Maeda, S.-I. I., Watanabe, S., Kanesaki, Y., Kobayashi, K., Nomata, J., Hanaoka, M., Watanabe, M., Ehira, S., Suzuki, E., Awai, K., and Nakamura, Y. (2017) CyanoBase: a large-scale update on its 20th anniversary. *Nucleic Acids Res.* **45**, D551–D554
57. Letunic, I., Doerks, T., and Bork, P. (2015) SMART: recent updates, new developments and status in 2015. *Nucleic Acids Res.* **43**, D257–60
58. Larkin, M. A., Blackshields, G., Brown, N. P., Chenna, R., McGettigan, P. A., McWilliam, H., Valentin, F., Wallace, I. M., Wilm, A., Lopez, R., Thompson, J. D., Gibson, T. J., and Higgins, D. G. (2007) Clustal W and Clustal X version 2.0. *Bioinformatics* **23**, 2947–8
59. Letunic, I., and Bork, P. (2016) Interactive tree of life (iTOL) v3: an online tool for the display and annotation of phylogenetic and other trees. *Nucleic Acids Res.* **44**, W242–5

TABLES

Table 1. Primer sets used in this study

Name	Sequence
DXCF-CBCRs	
Vector (pET28a)	Fw 5'-GGATCCGAATTCGAGCTC-3' Rv 5'-CATATGGCTGCCGCGCGG-3'
AM1_1378g	Fw 5'-CGCGGCAGCCATATGACCAACAAAATTCGCGCC-3' Rv 5'-CTCGAATTCGGATCCTCAGGCCATCGGTTGTTATT-3'
AM1_0048g1	Fw 5'-CGCGGCAGCCATATGATTGGTGAACCTCCATGTC-3' Rv 5'-CTCGAATTCGGATCCTCACTGCTGCAATTGATTGAC-3'
AM1_0048g2	Fw 5'-CGCGGCAGCCATATGACGCAATTAATCCGAGAA-3' Rv 5'-CTCGAATTCGGATCCTCAAGAGGTATTGGCAATCCA-3'
AM1_6305g1	Fw 5'-CGCGGCAGCCATATGACCAAAGAGATTCGGCAGAGT-3' Rv 5'-CTCGAATTCGGATCCTCACGTCTGTAATTCTTGCGAACG-3'
AM1_0829g	Fw 5'-CGCGGCAGCCATATGACCTACAAAATTAGGCAA-3' Rv 5'-CTCGAATTCGGATCCTCAAATCTGAGCTGTTGATG-3'
AM1_1870g4	Fw 5'-CGCGGCAGCCATATGATCTCCAAGATTCGAGAGTCC-3' Rv 5'-CTCGAATTCGGATCCTCACGCGTCAGCCGCTCCTT-3'
AM1_5997g4	Fw 5'-CGCGGCAGCCATATGGTTCGGCAAATTCGGCAA-3' Rv 5'-CTCGAATTCGGATCCTCAAACGGATAAAACATGACGTTG-3'
AM1_1870g4 mutant	
DGCF	Fw 5'-GTCAAAGACGGCTGTTTCCAAGATCGCTAT-3' Rv 5'-ACAGCCGTCTTTGACGTCATACCCCAA-3'
C ₇₅₄ S	Fw 5'-GGCGACTCTTTCCAAGATCGCTATACG-3' Rv 5'-TTGGAAAGAGTCGCCTTTGACGTCATA-3'
C ₇₈₂ S	Fw 5'-GATCCTTCTTATGTGGAGATGATGCAA-3' Rv 5'-CACATAAGAAGGATCTAAATTACAGGTGTT-3'
Phytochrome	
AM1_1870g1-g2	Fw 5'-CGCGGCAGCCATATGATGGATGTATCCTCCTCA-3' Rv 5'-CTCGAATTCGGATCCATCGCCGTCGACCGATGA-3'

Restriction sites are underlined.

Table 2. Peak absorbance wavelengths and binding efficiencies of DXCF CBCR GAF domains

	$\lambda_{\text{max, 15Z-isomer}}$ or $\lambda_{\text{max, dark-state}}$	$\lambda_{\text{max, 15E-isomer}}$ or $\lambda_{\text{max, photoproduct}}$	SAR
AM1_1378g	414	525	0.11
AM1_0048g1	418	498	0.75
AM1_0048g2	409	506	0.36
AM1_6305g1	557	491	1.4
AM1_0829g	417	579	0.32
AM1_1870g4			
WT	416	424	0.18
DGCF	425	420	0.34
C ₇₅₄ S	632	–	0.56
C ₇₈₂ S	410	–	0.13
C ₇₅₄ S/C ₇₈₂ S	595	–	0.05

n/a, not applicable

SAR, specific absorbance ratio, which was calculated as the peak absorption maximum of the 15Z-isomer or the dark state divided by the peak 280 nm absorption, providing a relative measure of chromophore-binding efficiency.

FIGURE LEGENDS

Figure 1. Phylogenetic tree of the CBCR GAF domains. The tree was constructed by the neighbor-joining method. The phytochrome GAF domains were selected as an outgroup. The CBCR GAF domains from *A. marina* were analyzed together with the DXCF CBCR GAF domains and the other typical CBCR GAF domains of the XRG, FR/X, and G/R lineages. All DXCF CBCR GAF domains from *Nostoc punctiforme* ATCC 29133 and *Anabaena* sp. PCC 7120, and the other typical DXCF GAF domains (SyPixJ1g2, TePixJg, SyCikAg, TeSesAg, and FdDpxAg) were included in this tree.

Figure 2. (A) Domain architecture of proteins including DXCF CBCRs from *A. marina*. Protein names are in accordance with CyanoBase. Domain definitions: TM: transmembrane region; GAF: cGMP-specific phosphodiesterases, cyanobacterial adenylate cyclases, and formate hydrogen lyase transcription factor FhIA; MA: methyl-accepting domain; HK: Histidine kinase domain; RR: response regulator domain; PAS: Per/Arnt/Sim domain; PHY: phytochrome-specific domain; HPT: Histidine phosphotransfer domain; CBS: cystathionine-beta-synthase. (B) Multiple sequence alignment of DXCF CBCRs from *A. marina* with TePixJg and TeSesAg.

Figure 3. SDS-PAGE of the purified proteins detected by staining with CBB (upper panels) and fluorescence imaging (lower panels). (A) DXCF-CBCR wild type proteins from *A. marina*. (B) DGCF variant of AM1_1870g4. (C) Canonical and second Cys mutant variants of AM1_1870g4. Solution photographs of the wild type and C₇₅₄S variant proteins are shown at the bottom.

Figure 4. Photoconversion of DXCF CBCRs from *A. marina*. (A) Absorption spectra of the blue-absorbing form (Pb, blue) and the green-absorbing form (Pg, orange) of AM1_1378g. (B) Absorption spectra of the blue-absorbing form (Pb, blue) and the teal-absorbing form (Pt, orange) of AM1_0048g1. (C) Absorption spectra of the blue-absorbing form (Pb, blue) and the teal-absorbing form (Pt, orange) of AM1_0048g2. (D) Absorption spectra of the green-absorbing form (Pg, blue) and the teal-absorbing form (Pt, orange) of AM1_6305g1. (E) Absorption spectra of the blue-absorbing form (Pb, blue) and the orange-absorbing form (Po, orange) of AM1_0829g.

Figure 5. Acid-denatured spectra of DXCF CBCRs from *A. marina*. (A) Absorption spectra of the blue-absorbing form (Pb, blue) and the green-absorbing form (Pg, orange) of AM1_1378g. (B) Absorption spectra of the blue-absorbing form (Pb, blue) and the teal-absorbing form (Pt, orange) of AM1_0048g1. (C) Absorption spectra of the blue-absorbing form (Pb, blue) and the teal-absorbing form (Pt, orange) of AM1_0048g2. (D) Absorption spectra of the green-absorbing form (Pg, blue) and the teal-absorbing form (Pt, orange) of AM1_6305g1. (E) Absorption spectra of the blue-absorbing form (Pb, blue) and the orange-absorbing form (Po, orange) of AM1_0829g.

Figure 6. Normalized Z-E difference spectra of native (A) and acid-denatured (B) proteins.

Figure 7. Difference spectra of the blue/teal (blue) and blue/orange (orange) photoconversions of AM1_0048g1 (A) and AM1_0048g2 (B).

Figure 8. Effects of IAM addition on AM1_6305g1. (A) Effect of IAM addition on the Pg form of AM1_6305g1. (B) Effect of IAM addition on the Pt form of AM1_6305g1. Green/teal (A) and teal/green (B) reversible photoconversions were observed 30 min after IAM addition.

Figure 9. Photoconversion of AM1_1870g4. (A) Absorbance spectra of dark-adapted AM1_1870g4 (blue) and after illumination with blue light (orange). (B) Photochemical difference spectrum of AM1_1870g4 (dark-adapted-photoproduct).

Figure 10. Photoconversion and dark-reversion kinetics of AM1_1870g4 at various temperatures. (A) Absorbance changes at 424 nm during photoconversion and dark-reversion cycles with different light intensities at 15°C, 20°C, 25°C and 30°C. (B) Correlation between light intensity and changes in absorbance (dark–light) at the temperatures shown in panel A. (C) Dark-reversion kinetics at temperatures the same as in panel A. (D) Arrhenius plot of AM1_1870g4. The parameter was calculated from the dark reversion kinetics at the different temperatures.

Figure 11. Acid-denatured spectra of AM1_1870g4. (A) Denatured spectra of the dark-adapted form before (blue) and after (orange) light illumination. (B) Denatured spectra of the photoproduct before (blue) and after (orange) light illumination. (C) Denatured spectra of the dark-adapted form (blue) and the photoproduct (orange) before light illumination. (D) The *Z–E* difference spectrum.

Figure 12. Swapping the Asp residue of the GDGF motif with the next Gly residue. (A) Dark-adapted (blue) and light-illuminated (orange) spectra of AM1_1870g4-DGCF. (B) The difference spectrum of photoconversion of AM1_1870g4-DGCF.

Figure 13. Acid-denatured spectra of AM1_1870g4-DGCF. (A) Denatured spectra under the dark condition before (blue) and after (orange) light illumination. (B) Acid-denatured spectra of AM1_1870g4-DGCF under blue light illumination before (blue) and after (orange) light illumination. (C) The difference spectra of denatured AM1_1870g4-DGCF before and after white light illumination.

Figure 14. Site-directed mutagenesis of the canonical and second Cys residues of AM1_1870g4. (A) Absorption spectra of the dark-adapted (blue) and light-illuminated (orange) C₇₅₄S variant of AM1_1870g4. (B) Absorption spectra of the dark-adapted (blue) and light-illuminated (orange) C₇₈₂S variant of AM1_1870g4. (C) Absorption spectra of the dark-adapted (blue) and light-illuminated (orange) C₇₅₄S/C₇₈₂S variant of AM1_1870g4.

Figure 15. Acid-denatured spectra of the C₇₅₄S, C₇₈₂S, and C₇₅₄S/C₇₈₂S variants. (A) Acid-denatured spectra of the C₇₅₄S variant before (blue) and after (orange) white light illumination. (B) Acid-denatured spectra of the C₇₈₂S variant before (blue) and after (orange) white light illumination. (C) Acid-denatured spectra of the C₇₅₄S/C₇₈₂S variant before (blue) and after (orange) white light illumination. (D) Photochemical difference spectra of the C₇₈₂S variant (blue) and covalently bonded PCB (orange, AnPixJg2).

Figure 16. Photoconversion of phytochrome region of AM1_1870 (AM1_1870g1-g2). Absorption spectra of the red-absorbing form (Pr, blue) and the far-red-absorbing form (Pfr, orange). Inset: SDS-PAGE of the purified AM1_1870g1-g2 detected by staining with CBB (left gel) and fluorescence imaging (right).

Figure 1

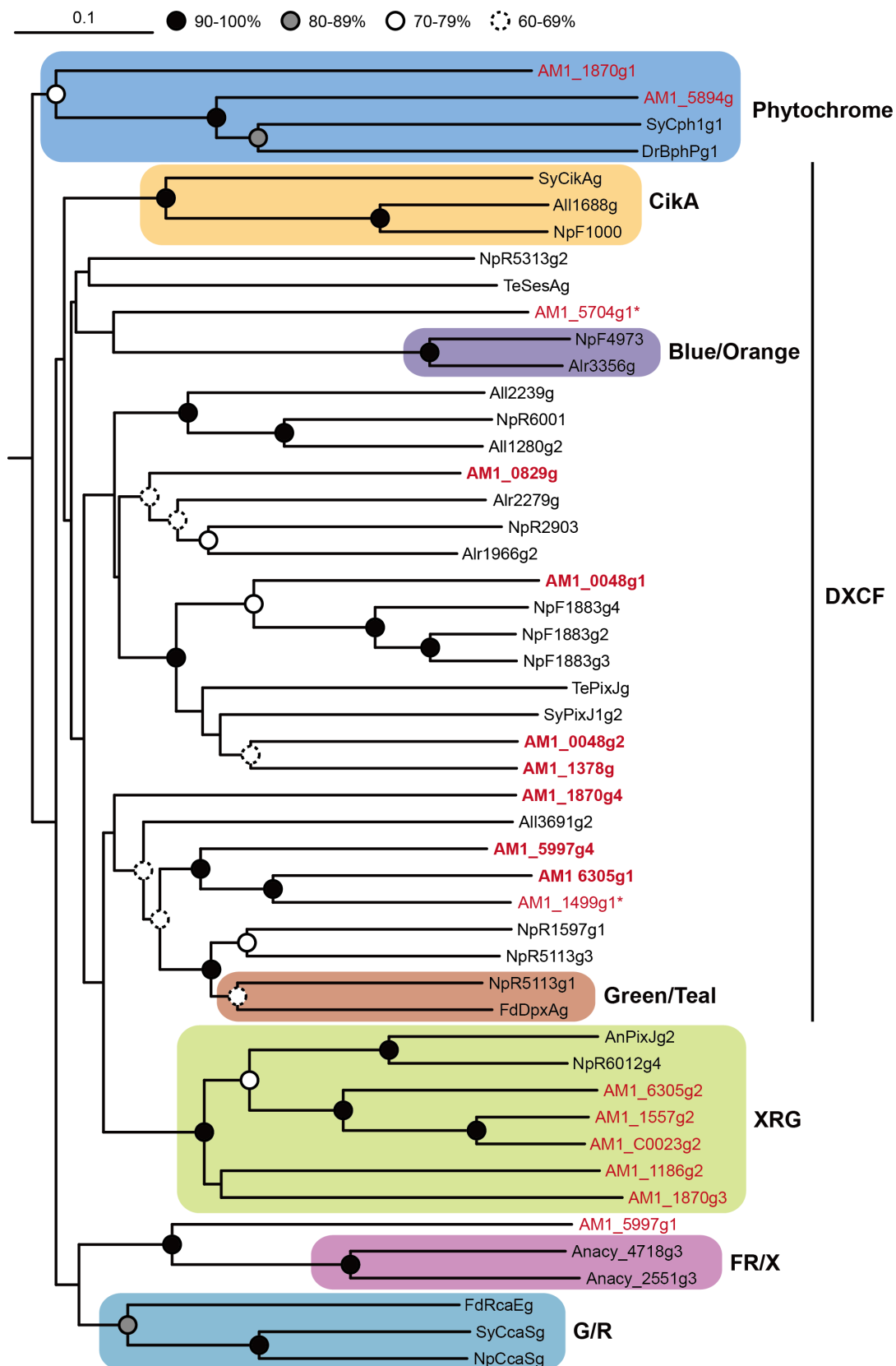
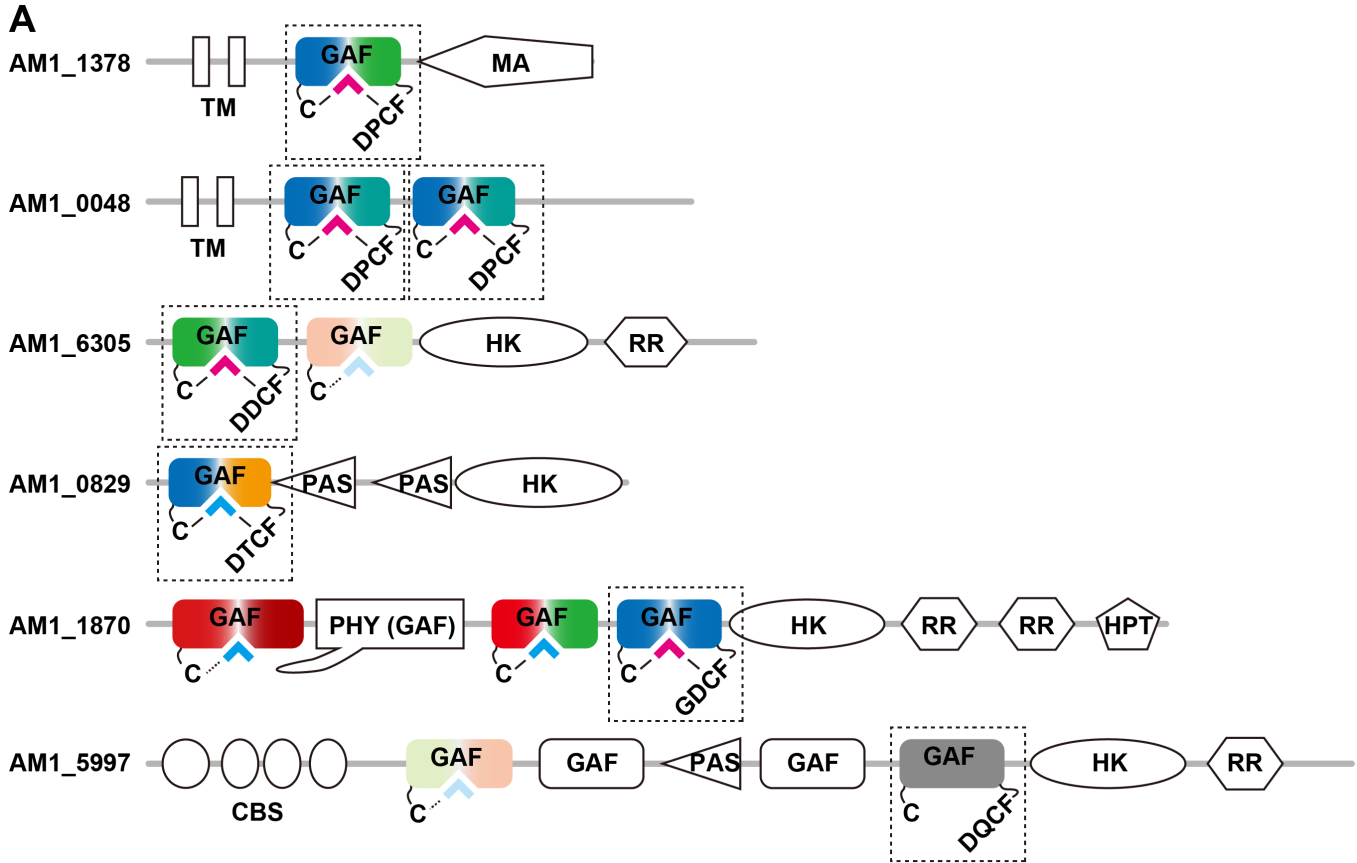


Figure 2



B

	DRQAIFETLVAKGRELLACDRVIVYAFDDNY---VGTVVAESVAEGWPQARDQVIEDPCF	REHWVEAYRQGR	IQATTD
TePixJg	DRQAIFETLVAKGRELLACDRVIVYAFDDNY---VGTVVAESVAEGWPQARDQVIEDPCF	REHWVEAYRQGR	IQATTD
TeSesAg	RLEEILQRAVNSIQQLLSDRVLIYRFLGD---GSCIVAVEATTLPQYSILGQVIHDP	CF	TKETARRFLEGR
AM1_1378g	NEDDVLNTTVEEARKIKADRVIVYGFDEDW---YGTVIAESAIPGIKALWAEIKDPC	FAENYVEKYRAGR	IQAINN
AM1_0048g1	SEEDLLKTTVAEVRQILQTDRTVIFALNNG---ECTFVAESVAPGPKLQWSTLHDP	CF	NEGYQEQYRQGRVSAIDN
AM1_0048g2	HTEEILTNAVQESRKVLRADRVIVYSFDENW---QGTVAAEAVQPGISKMWAEISD	PCF	FANKYVEQYRRGRVQAINN
AM1_6305g1	ETQTIFFETSVQRVLELIKANRVAIFKLDSATNYTTCFV	AEKVVPPFTSALAANVRDDCF	GHNYANKYQQQVFAVAD
AM1_0829g	DLHEILQTTVTEVRQLLDADRVVMFQIHPDG---ACTVVQEA	VLPGWSKSI	NQNI
AM1_1870g4	DLETIFKTTTREVRLQVDRVVVFQFLPDVQYSQGEVIAEDVHPD	YRSILGYDVKGDC	CFQDRYTASPGTHQVFAIDD
AM1_5997g4	EPQLIFRTAVTQVRKLLAVDRVCIYRFIEDAGYSQGM	MAEEVLP	PEFPSALTAQVRDQCF
		GDEYATQY	QNGRFQAVAD
TePixJg	IFKAGLTECHLNQLRPLKVRANLVVPMVIDDQLFGLL	IAHQ	CEPRQWQEI
TeSesAg	VNQAQLQDCYRELLTRLQVQANLVVPLQGHQHLWGLL	IAHCRSPRLWQREELFLLQRIA	EPLTVALQQAEMYEALE
AM1_1378g	VHEAGLTKCHLAQLEPFQKANLVVPIILREEKLFGLL	IAHQ	TQPRVQWQESI
AM1_0048g1	IYNSGLNDCHIGLLERFAVKANIVAPILQENENLYGLL	IAHQ	CARPREWQSEI
AM1_0048g2	VNDAGLTECHVQOLEKYVQANLVVPIVGEYLFGLL	IAHQ	CSGPRIWQSEI
AM1_6305g1	IYAENLSDCHVRIERFQVRANLVVPLQGEKLWGLL	CIHQ	CSGPRAWQPYETQFI
AM1_0829g	IETAPITPCHADLLRQFEVKANLVPIIISQQLWGLL	IAHQ	SAPREWQAFV
AM1_1870g4	LNTCNLDPCYVEMMQGLVQAHLVVPLFRSNIWGLL	IAHQ	SAPRPWQVKERFAIQI
AM1_5997g4	IYDAGLSECHIEILDLFHIRANLVVPLQGDNLWGLL	CIHQ	SGPRSQWQDEIEFVQKIANQLGIALYQAEILLKEQ

DXCF motif

↑
Canonical Cys

Figure 3

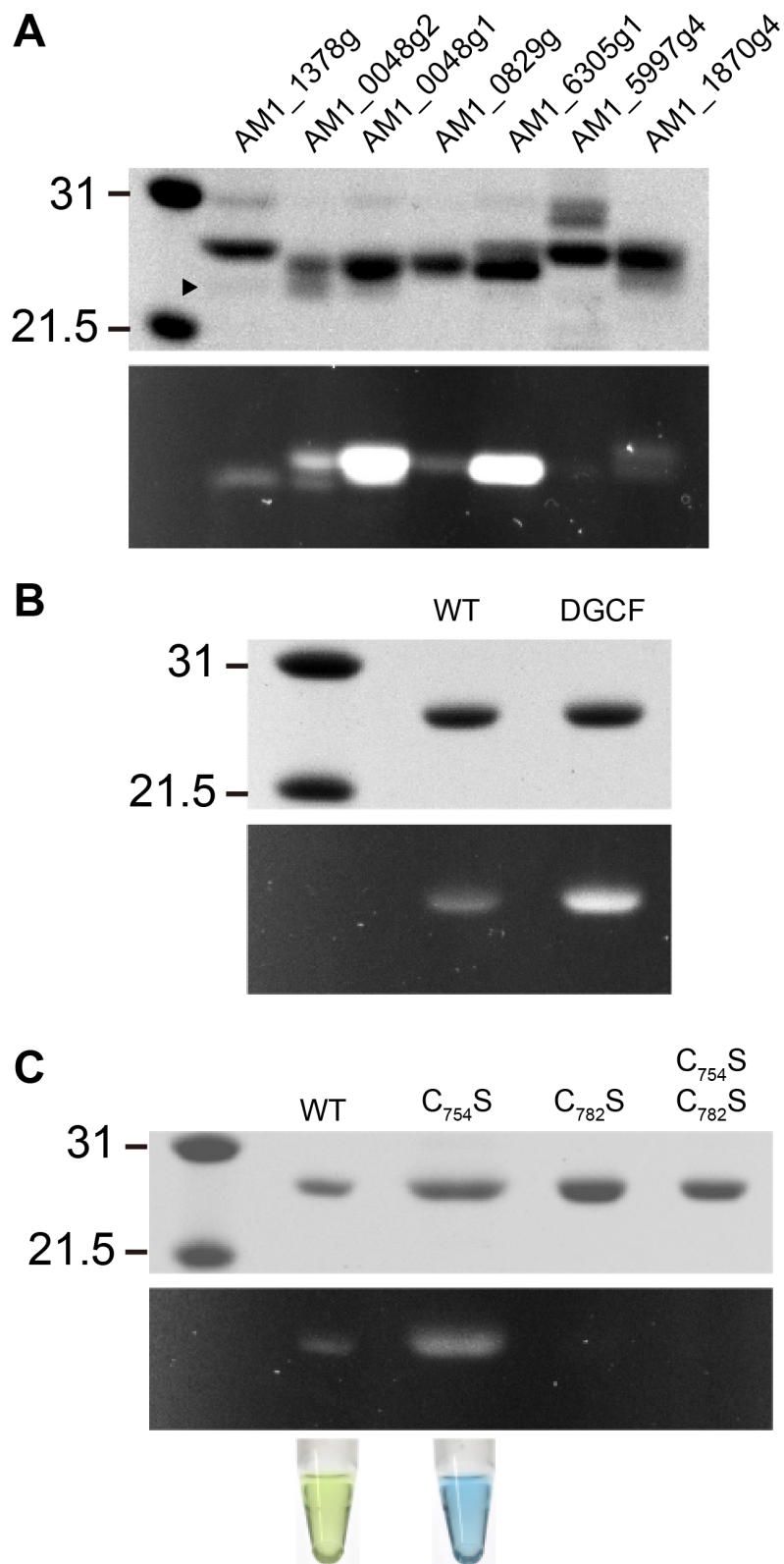


Figure 4

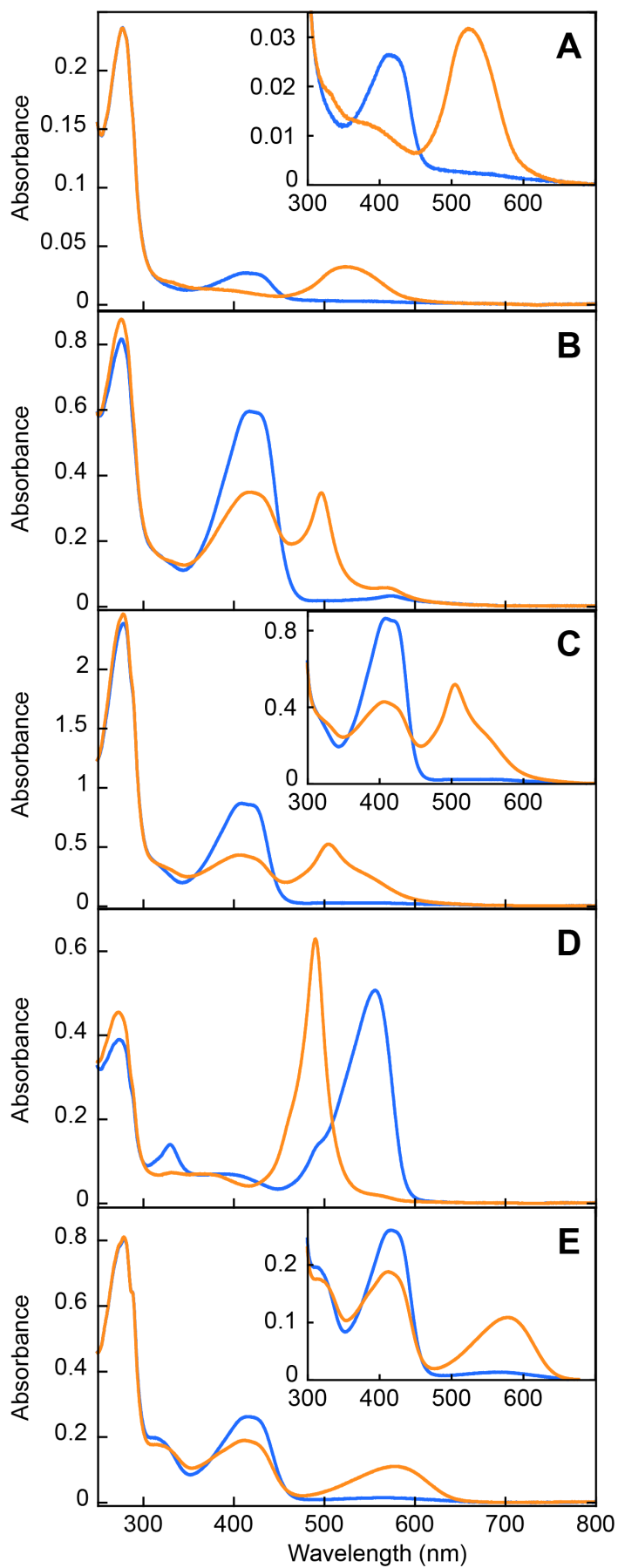


Figure 5

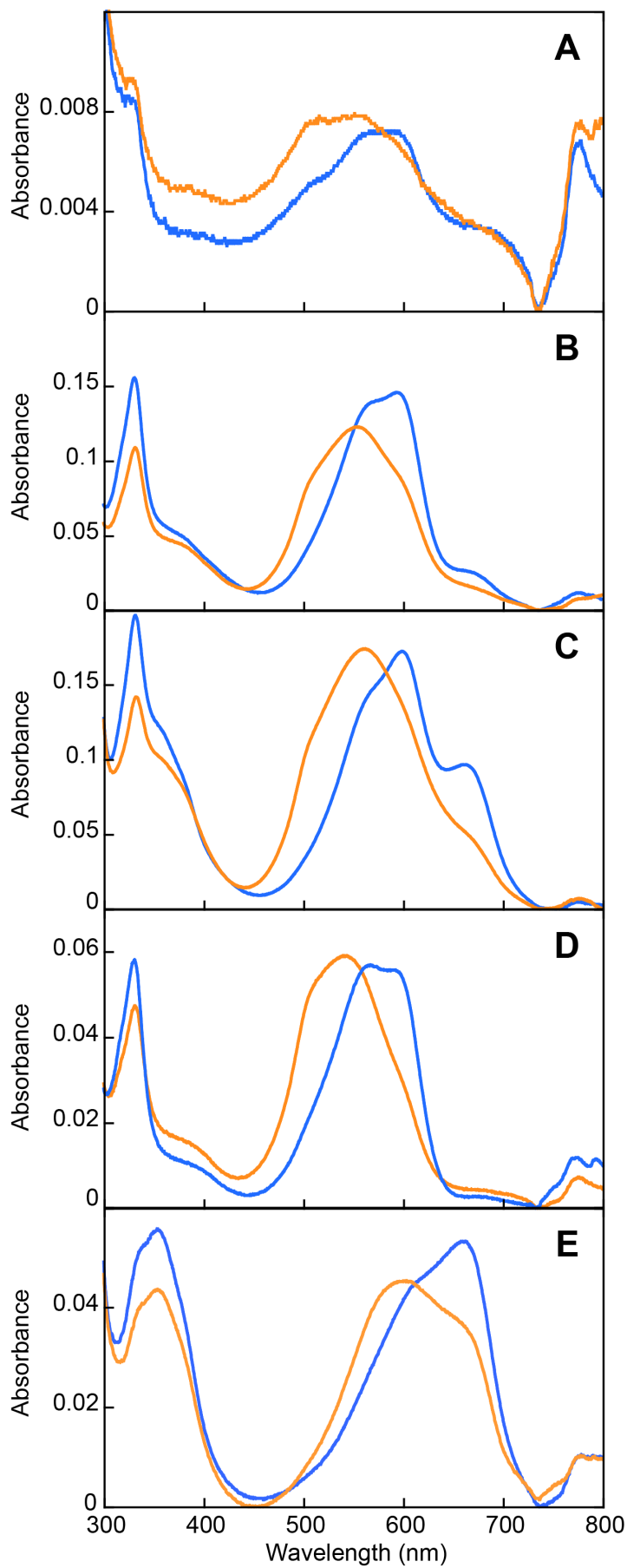


Figure 6

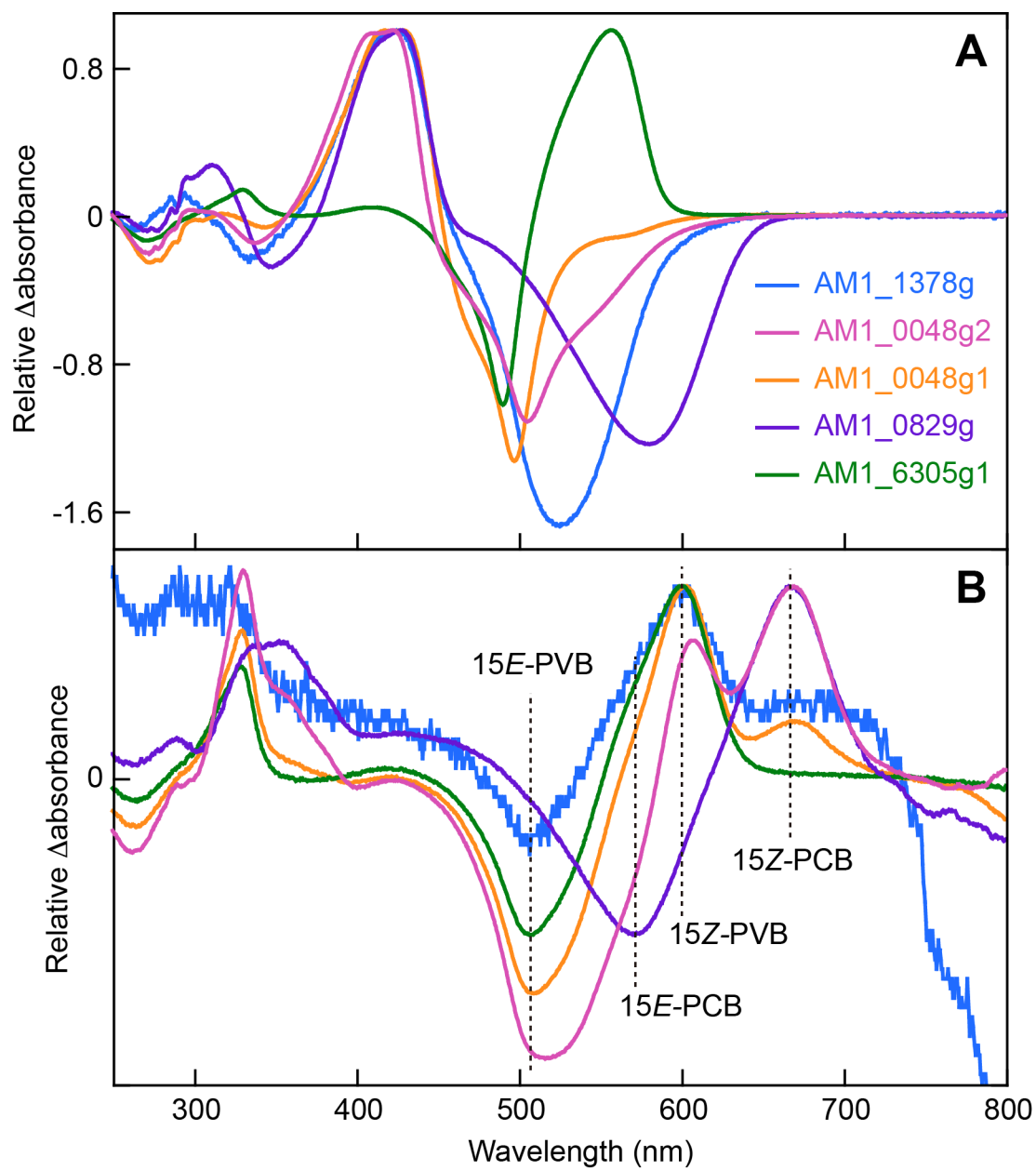


Figure 7

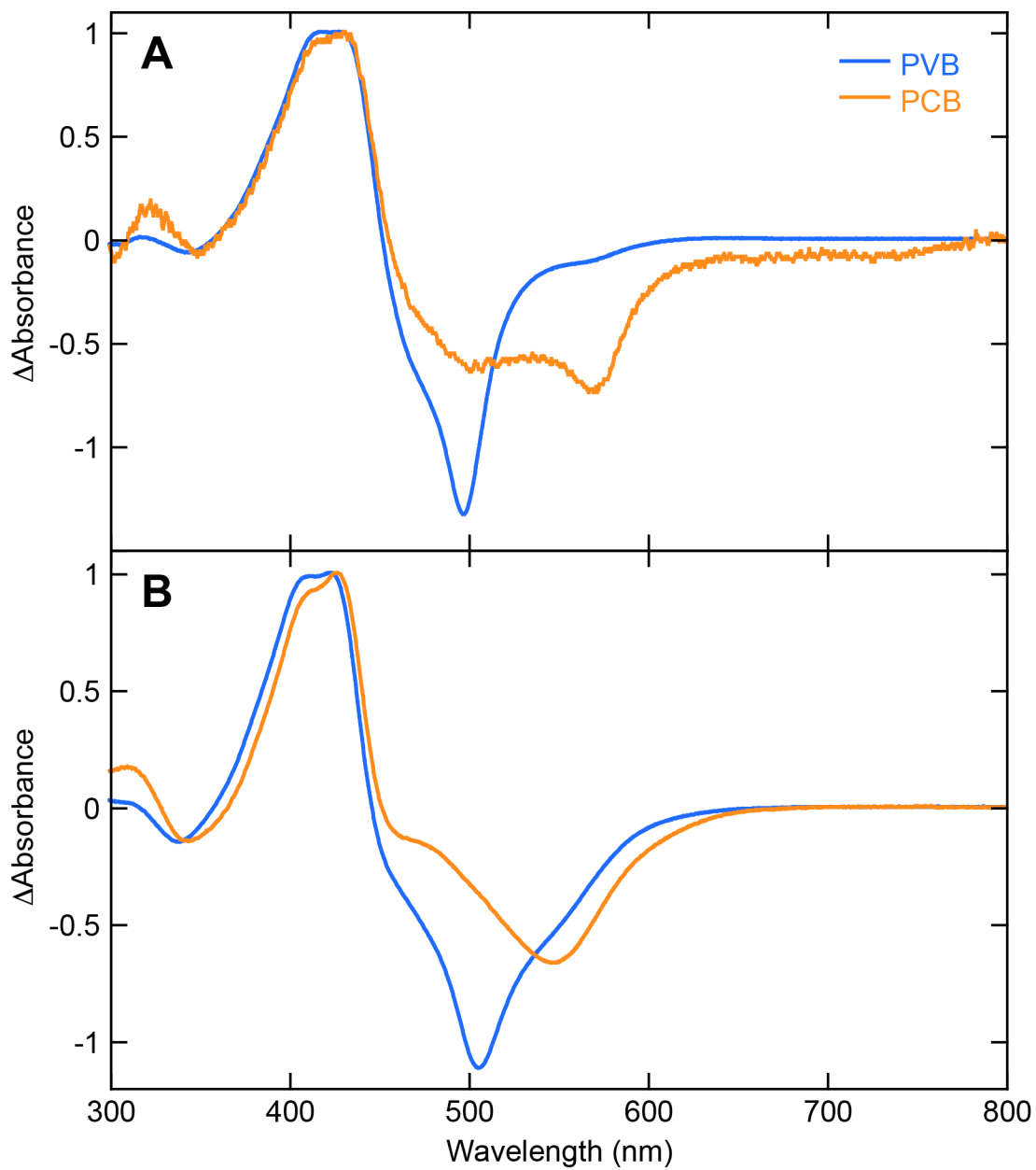


Figure 8

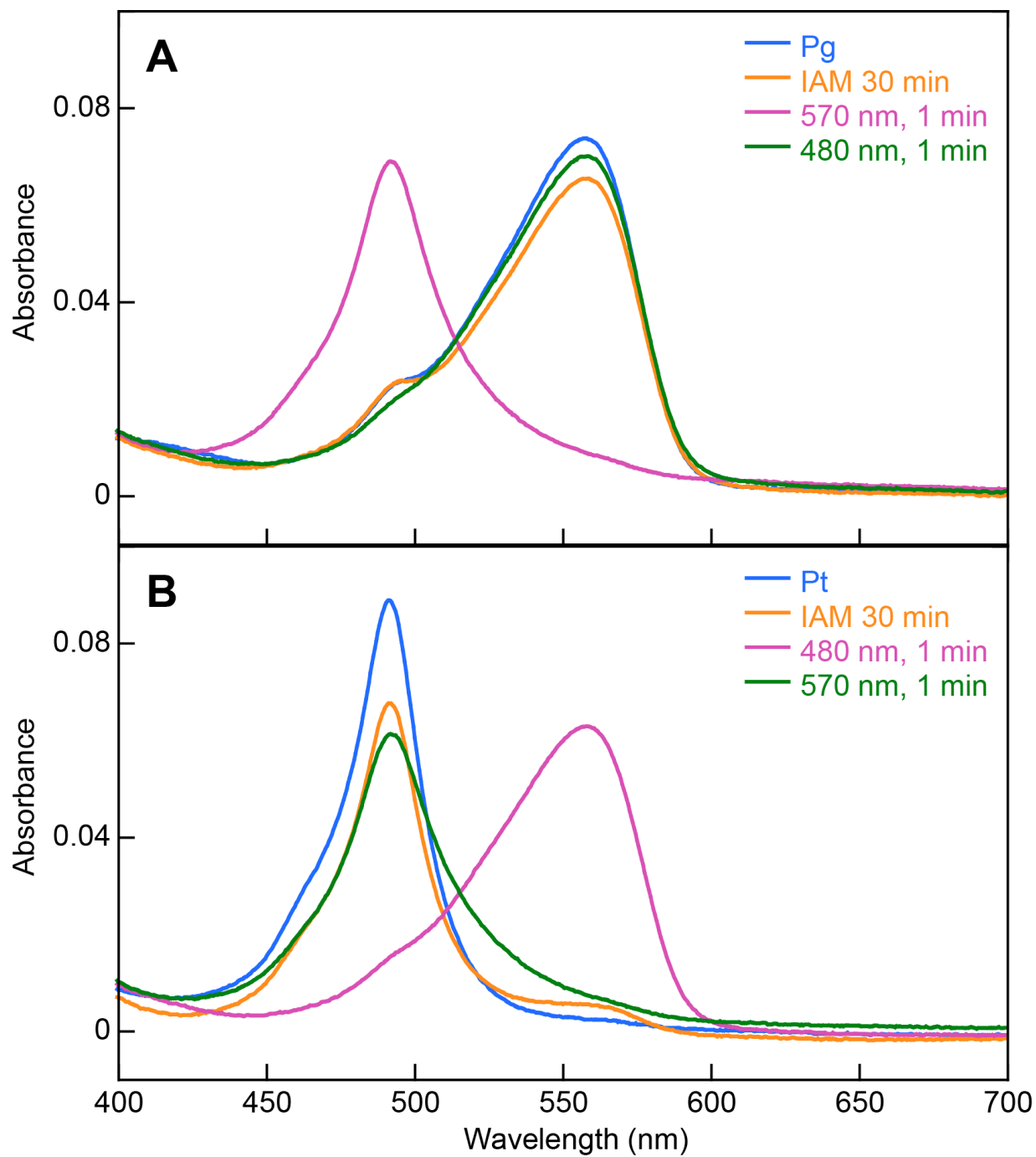


Figure 9

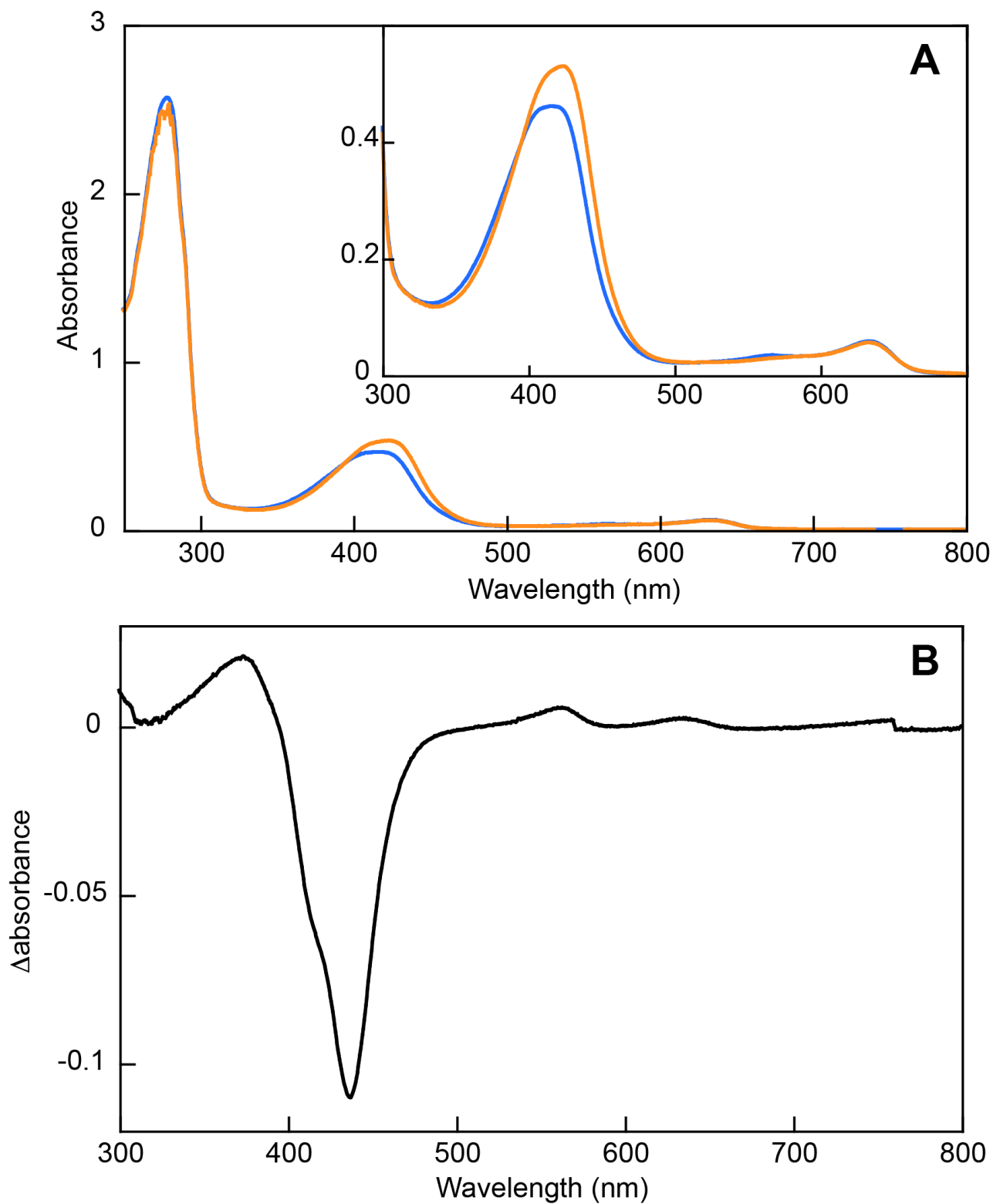


Figure 10

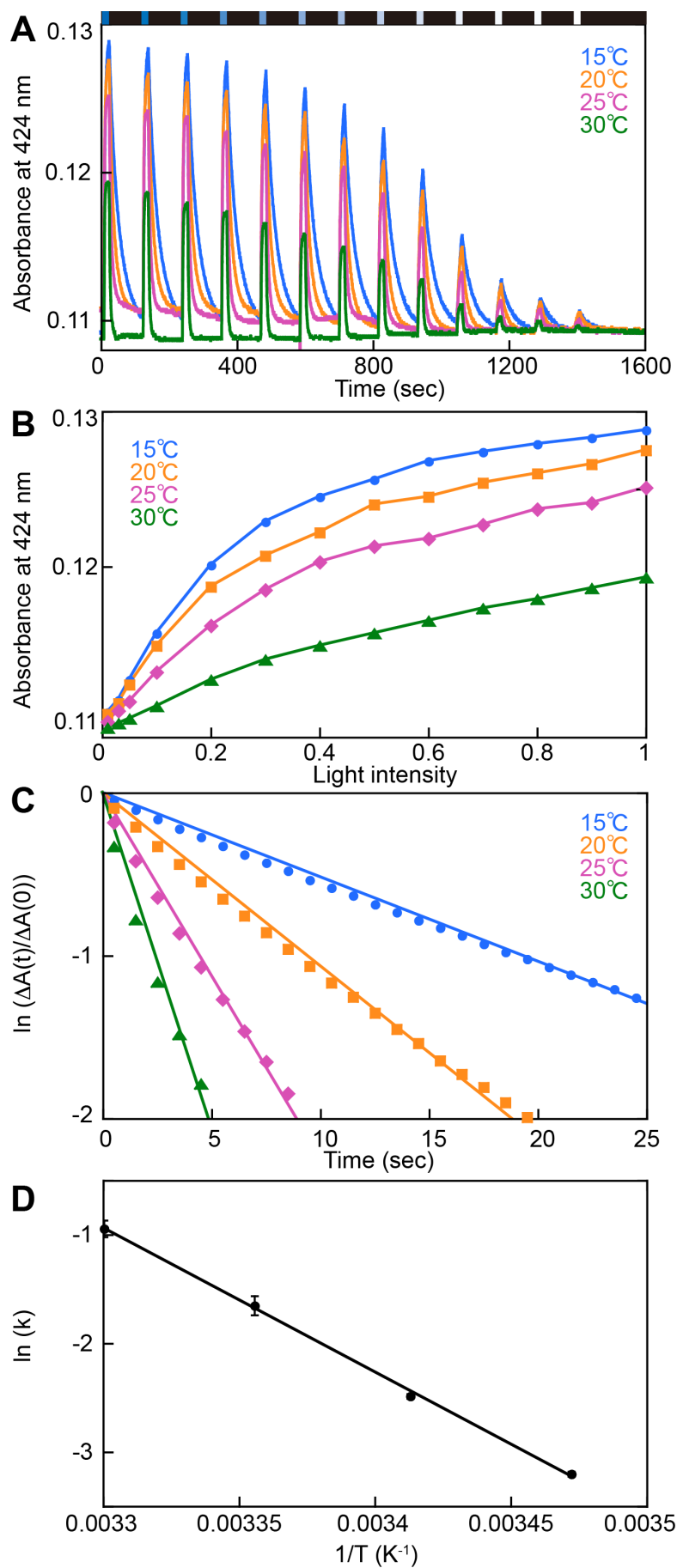


Figure 11

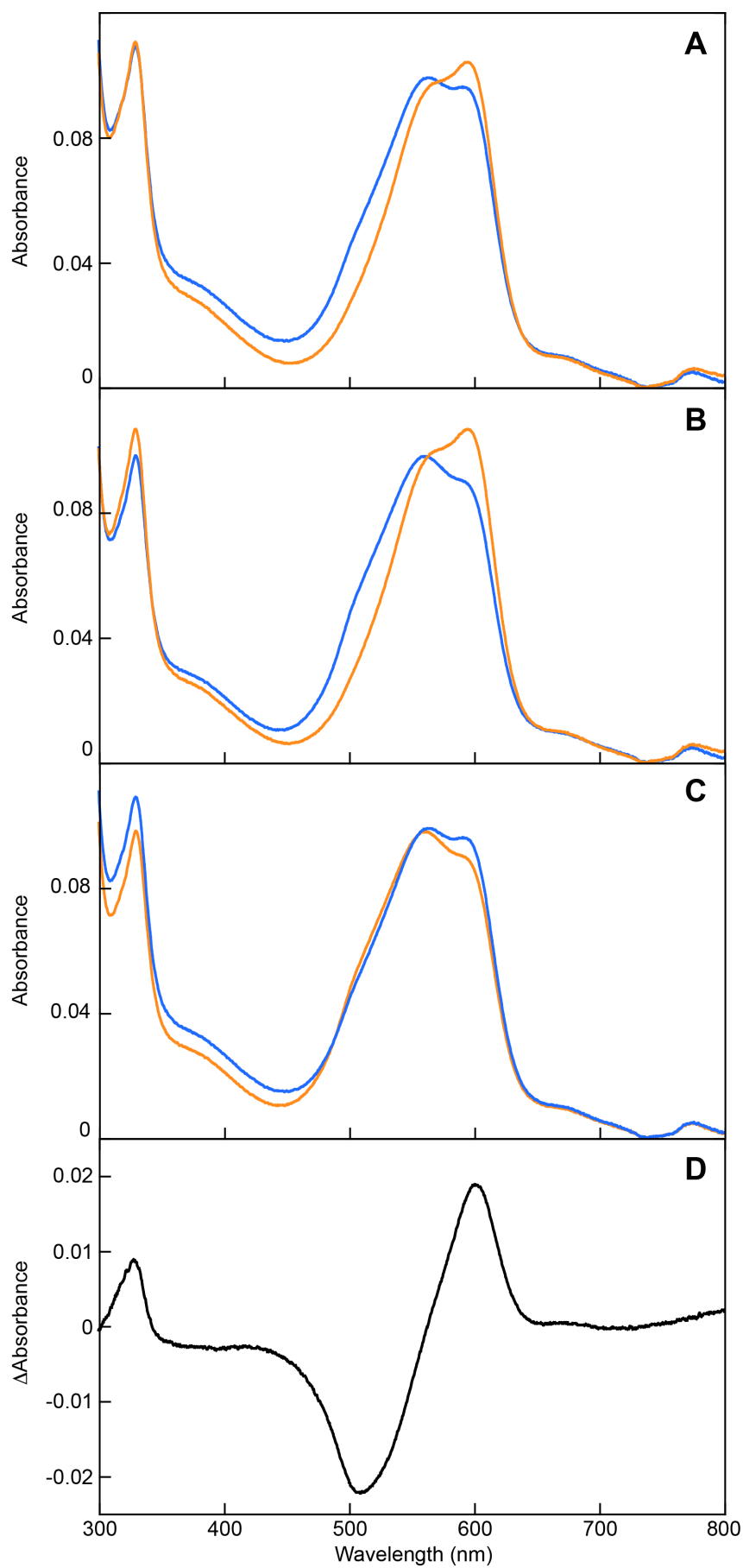


Figure 12

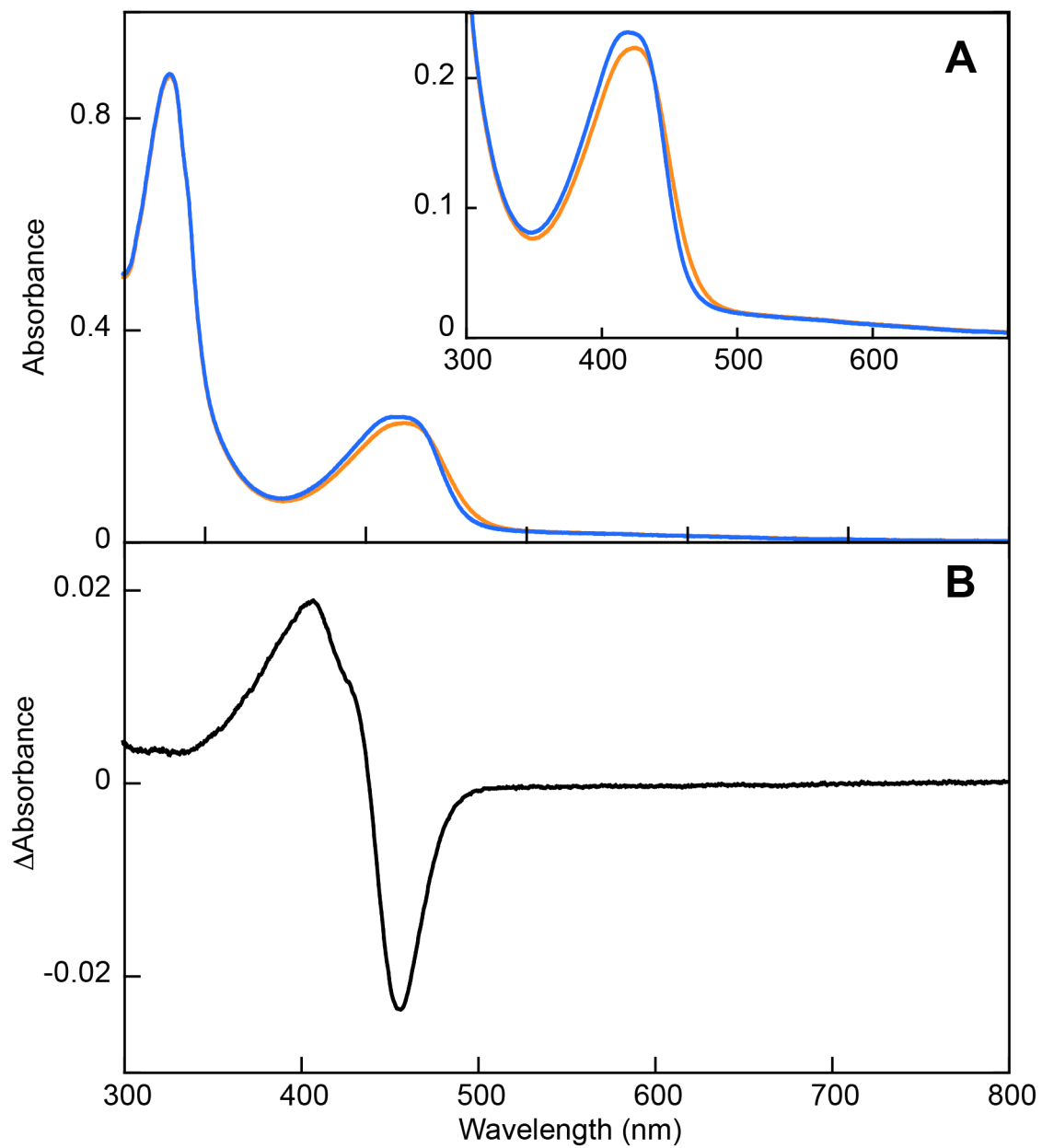


Figure 13

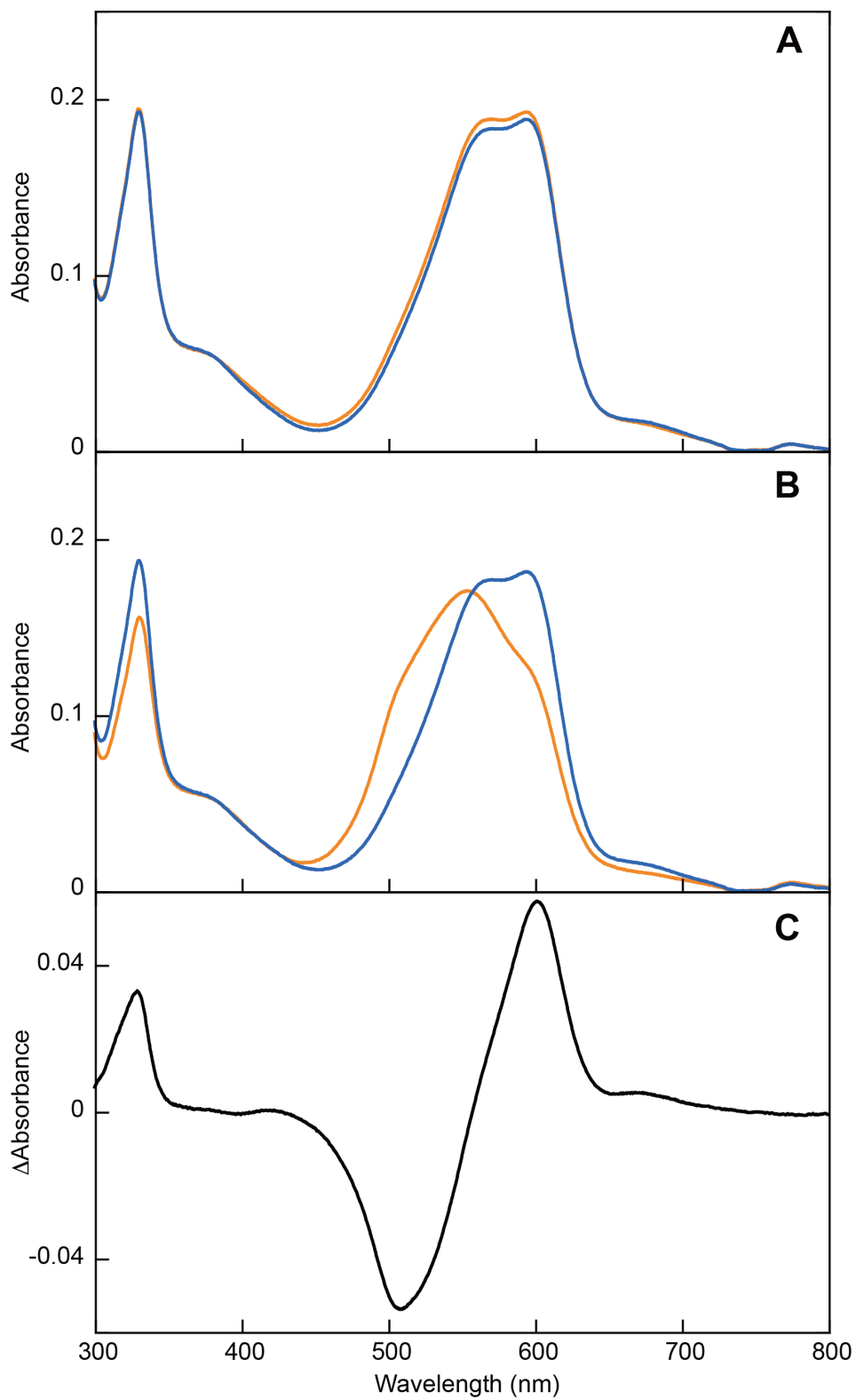


Figure 14

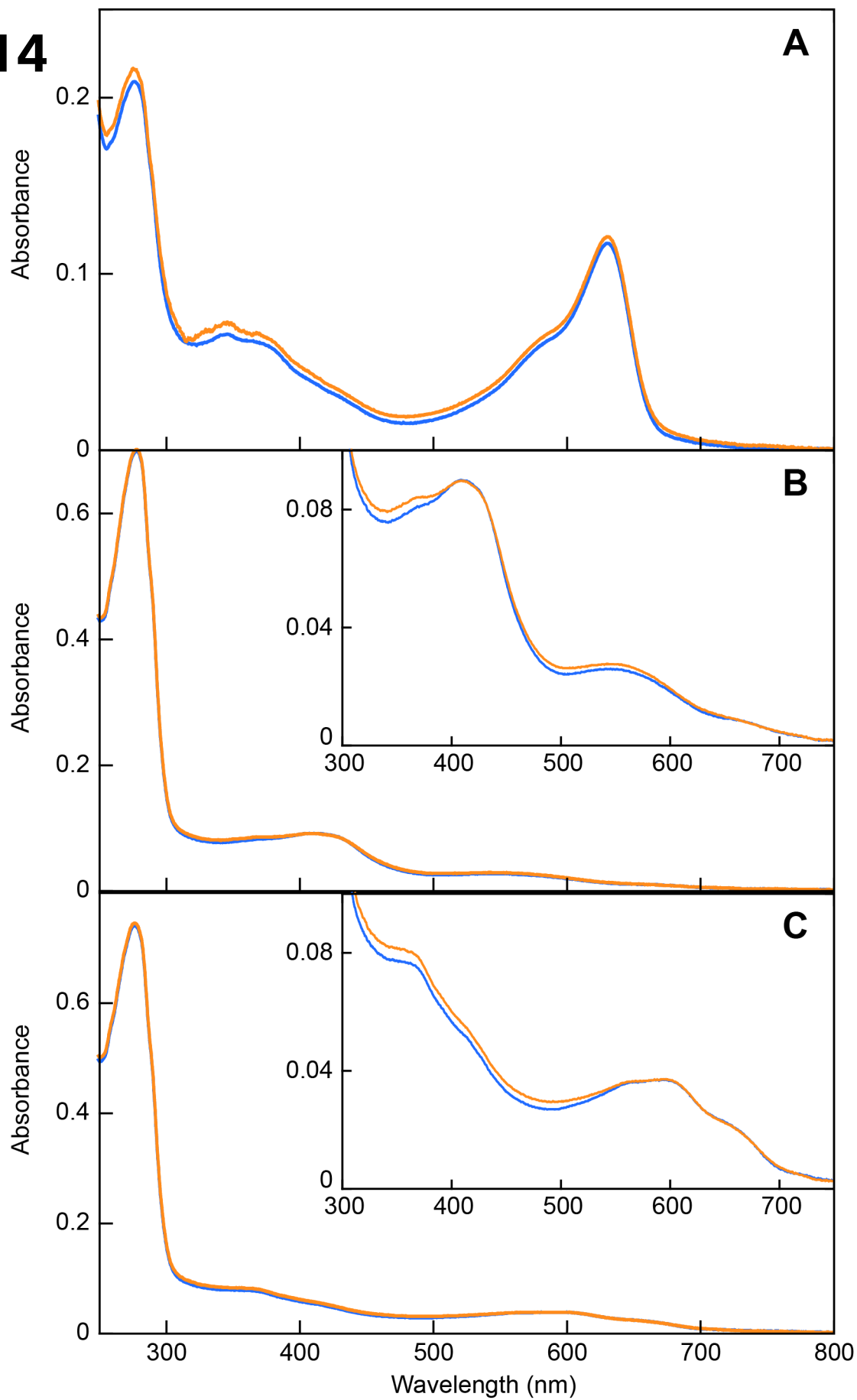


Figure 15

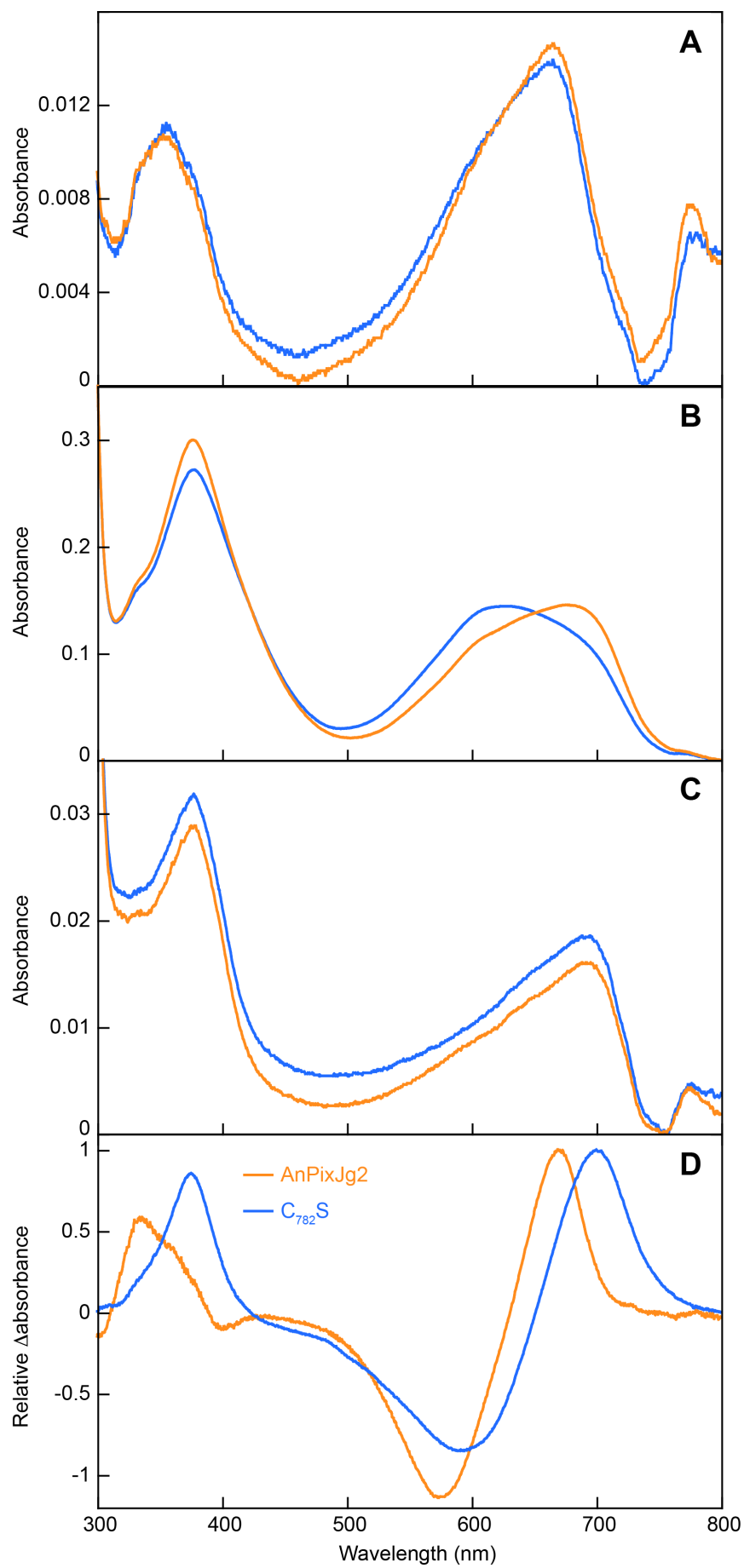
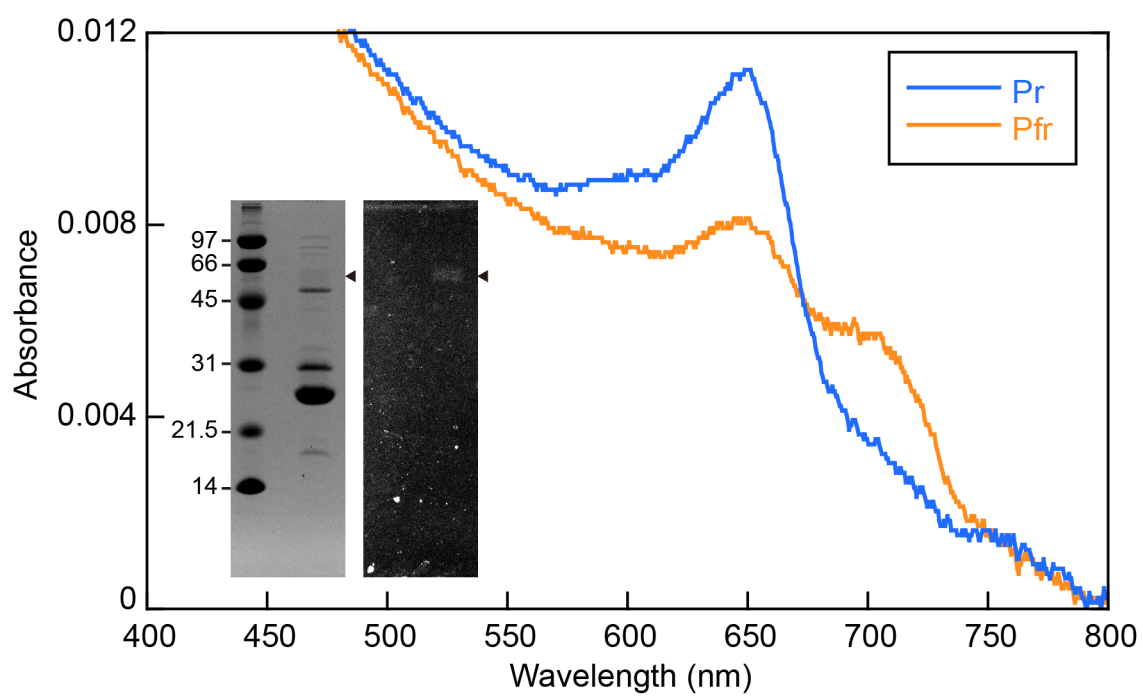


Figure 16



**Molecular characterization of DXCF cyanobacteriochromes from the cyanobacterium
Acaryochloris marina identifies a blue-light power sensor**

Masumi Hasegawa, Keiji Fushimi, Keita Miyake, Takahiro Nakajima, Yuki Oikawa, Gen
Enomoto, Moritoshi Sato, Masahiko Ikeuchi and Rei Narikawa

J. Biol. Chem. published online December 11, 2017

Access the most updated version of this article at doi: [10.1074/jbc.M117.816553](https://doi.org/10.1074/jbc.M117.816553)

Alerts:

- [When this article is cited](#)
- [When a correction for this article is posted](#)

[Click here](#) to choose from all of JBC's e-mail alerts